HIV-induced membraneless organelles orchestrate post-nuclear entry steps.

Viviana Scoca[1], Renaud Morin[2], Jean-Yves Tinevez[3], Francesca Di Nunzio[1]

[1]Department of Virology, Advanced Molecular Virology Unit, Université de Paris, F-75015 Paris, France
[2] Imactiv-3D, 1 Place Pierre Potier, 31106 Toulouse,
[3] Image Analysis Hub/ C2RT, Institut Pasteur, Université de Paris, F-75015 Paris, France

Running title: Running title: HIV-1 prompts virus-MLOs formation by liquid-liquid phase separation.

Abstract

HIV integration occurs in chromatin sites that favor the release of high levels of viral progeny, alternatively the virus is also able to coexist discreetly with the host. The viral infection perturbs the cellular environment inducing the remodeling of the nuclear landscape. Indeed, HIV-1 triggers the nuclear clustering of the host factor CPSF6, but the underlying mechanism is poorly understood. Our data indicate that HIV usurps a recently discovered biological phenomenon, called liquid-liquid phase separation (LLPS), to hijack the host cell. We observed CPSF6 clusters as part of HIV-induced membraneless organelles (HIV-1 MLOs) in macrophages, which are one of the main HIV target cells. We describe that HIV-1 MLOs follow phase separation rules and represent functional biomolecular condensates. We highlight HIV-1 MLOs as hubs of nuclear reverse transcription, while the double stranded viral DNA, once formed, rapidly migrates outside these structures. Transcription-competent proviruses localize outside but near HIV-1 MLOs, in LEDGF-abundant regions, known to be active chromatin sites. Therefore, HIV-1 MLOs orchestrate viral events prior to the integration step and create a favorable environment for the viral replication. This study uncovers single functional host-proviral complexes in their nuclear landscape, which is markedly restructured by HIV-1 to favor viral replication.

Introduction

Immediately after fusion at the plasma membrane, HIV-1 cores are released into the cytoplasm and move towards the nucleus, while the viral RNA (vRNA) genome begins the process of reverse transcription (RT) into double-stranded viral DNA (ds vDNA)(Blanco-Rodriguez and Di Nunzio, 2021; Campbell and Hope, 2015; Di Nunzio, 2013; Scoca and Di Nunzio, 2021). Once imported in the nucleus, the interplay between the HIV-1 DNA genome and the host chromatin compartment is crucial for the fate of the virus-host coexistence. Recent discoveries in early steps of HIV life cycle (Blanco-Rodriguez et al., 2020; Burdick et al., 2020; Dharan et al., 2020; Li et al., 2021; Rensen et al., 2021; Selyutina et al., 2020; Zila et al., 2021) revise the commonly accepted models of uncoating (loss of the viral capsid) and reverse transcription as exclusive cytoplasmic processes (Farnet and Haseltine, 1991; Suzuki and Craigie, 2007). It has been found that HIV prompts clusters of the Cleavage and Polyadenylation Specificity Factor Subunit 6 (CPSF6) proteins outside the paraspeckles, but in co-localization with some nuclear speckle factors (Francis et al., 2020; Rensen et al., 2020). However, the nature, the behavior and the underlying mechanism behind the establishment of these organelles are still unknown.

Here, we distinguish the topological duplicity of the post-nuclear viral entry phases: the early and the late. Early post-nuclear entry steps involve the formation of the HIV–induced membraneless organelles (HIV-MLOs), composed by CPSF6 clusters enlarged with viral factors. Late post-nuclear entry steps are characterized by the completion of the double-stranded vDNA synthesis. The final products of the reverse transcription process are recruited into the pre-integration complex (PIC) eventually for viral integration and transcription. The vDNA nuclear dynamics and its surrounding chromatin landscape dictate the evolution of HIV infection (Maldarelli, 2016; Sharkey et al., 2011; Sharkey et al., 2000). However, the mechanisms behind the fate of the proviral DNA in the nucleus remain unclear (Liu et al., 2020; Olson et al., 2019). These are challenging to study, also due to the limits imposed by available technologies. Real-time imaging approaches can provide new insight into unprecedented spatial information in single cells by tracking individual viruses.

Here, we perform single cell study. We describe early post-nuclear entry steps in which the viral infection enhances the phase separation of CPSF6, building HIV-1 MLOs. Our

results emphasize post nuclear entry steps as finely regulated by the interplay between viral and host components. Of note, CPSF6 contains intrinsically disordered mixed-charge domains which are responsible for the formation of liquid condensates *in vitro* (Greig et al., 2020) and they may account for the formation of HIV-1 MLOs in infected cells. Membraneless organelles are established through a recently discovered biological phenomenon called liquid-liquid phase separation (LLPS) in which molecules transition from a liquid state to a more solid state, similarly to oil and water demixing (Alberti et al., 2019; Banani et al., 2016). Our data reveal that HIV-1 MLOs undergo biomolecular condensates' rules, concentrating viral and host factors in the same niche and hosting nuclear reverse transcription.

For the study of the late post-nuclear entry steps, we labelled the newly synthesized ds vDNA through the HIV-1 ANCHOR system (Blanco-Rodriguez et al., 2020). The ds vDNA is the only form included in the mature PIC able to give rise to a functional infection. Through the tracking of the vDNA and transcriptional vRNA we found that transcriptional viral foci are excluded, but remain in the vicinity of HIV-1 MLOs. Our finds suggest HIV-1 MLOs' role in creating a surrounding microenvironment favorable for viral replication. We provide new insights into how HIV reprograms and markedly restructures the nuclear environment to orchestrate viral replication steps.

Results

CPSF6 clusters are hubs of viral reverse transcription.

Upon nuclear entry, the virus reprograms the nuclear localization of the host Cleavage and Polyadenylation Specificity Factor Subunit 6 (CPSF6) from being randomly dispersed in the nucleoplasm to discrete clusters (Fig. 1A)(Bejarano et al., 2019; Francis et al., 2020; Rensen et al., 2021). It has been suggested that the nuclear entry of the viral capsid that interacts with CPSF6 (Buffone et al., 2018; Price et al., 2014) could drive the formation of CPSF6 clusters (Francis et al., 2020). On the other hand, this phenomenon could also be prompted by the overexpression of CPSF6 (Chaudhuri et al., 2020) due to the viral infection.

Here, we characterize the HIV-1 post-nuclear step and its interplay with the host nuclear landscape in human macrophages. First, we evaluated the nuclear location of

the viral endogenous integrase (IN) protein by the immuno-labelling of the hemagglutinin (HA) tag fused to the C-terminal domain of the IN (Blanco-Rodriguez et al., 2020; Petit et al., 2000). We confirmed that the majority of the viral IN proteins accumulate in foci occupied by CPSF6 clusters (Fig. 1A)(Francis et al., 2020; Muller et al., 2021; Rensen et al., 2021). To better define the relevance of these viral-host clusters, we performed an immuno-RNA smiFISH (single molecule inexpensive FISH) (Rensen et al., 2021), specific for HIV-1, and we uncovered the presence of incoming viral RNA (vRNA) inside CPSF6 clusters (Fig. 1B). Upon the block of reverse transcription through Nevirapine (NEV) treatment, we observed incoming vRNA genomes 100% located inside CPSF6 clusters. Likewise, in physiological infection conditions at 48h post-infection, without the drug treatment, vRNA foci can be detected inside CPSF6 clusters (Fig. 1B) in most of the cells. Only few cells showed a mixed population of vRNA foci inside and outside, suggesting that the detected vRNAs can have a different nature (Fig. 1B). Thus, we asked the functional role of the co-existence between the incoming vRNA and IN proteins sequestered inside CPSF6 clusters. We performed in infected and uninfected macrophage-like cells, chromatin immunoprecipitation (ChIP) of the endogenous CPSF6 protein followed by real-time PCR (Fig. 1C, Fig. S1). Early, intermediate, and late reverse transcription (RT) products were amplified using appropriate primers. The data revealed an “ongoing” RT inside CPSF6 clusters, and, interestingly, early transcripts were more abundant than the others (Fig. 1C). Our results explain previous data showing EdU-labeled vDNA forms clustering in nuclear niches in macrophages (Francis et al., 2020; Rensen et al., 2020), indicating that they serve as hubs of nuclear RT. We called these host/viral nuclear niches HIV-induced membraneless organelles (HIV-1 MLOs).

HIV-1 MLOs are phase separated condensates

Eukaryotic cells evolved organelles without membrane (membraneless organelles (MLOs)) to allow the fine regulation of complex functions in a spatiotemporal manner. Biomolecular condensates are dynamic and reactive (Banani et al., 2016) and their composition is heterogeneous, usually involving a mixture of proteins and nucleic acids (Fare et al., 2021). The newly characterized liquid-liquid phase separation (LLPS) phenomenon governs MLOs formation. LLPS can be driven by the spontaneous assembly of intrinsically disordered regions (IDRs) present in some proteins (Li et al., 2012), separating from the cellular milieu.

HIV prompts the redistribution of CPSF6 in the nucleus from randomly distributed to aggregation in clusters. Intriguingly, we observed an increase in CPSF6 intensity exclusively in the nucleus of infected cells (Fig.2A), in line with a recent study from Chandravanu's laboratory (Chaudhuri et al., 2020).

LLPS droplets form through the process of nucleation and growth, until large enough to overcome surface tension. They can maintain a critical radius to be stable and continue to grow (Strom and Brangwynne, 2019). We find that CPSF6 clusters increase twice their volume along the time post-infection (24h p.i. vs.72h p.i.) and that they are spherical (Fig.2B), typical shape of liquid droplets. The mean intensity of IN signal inside HIV-1 MLO positively correlates with the mean intensity of CPSF6 (Pearson's r= 0.8563) (Fig. S2A), indicating that HIV-1 MLOs undergo phase separation rules. Next, to live-track virus-induced CPSF6 clusters and to investigate their behavior, we used differentiated THP-1 cells stably expressing CPSF6 fused to mNeonGreen. We performed time-lapse epifluorescence microscopy at 5-min intervals to capture fusion events (Fig. 2C, video 1). We could appreciate the high dynamism of the MLOs (Fig. S2B), which keep restoring their circular shape (Fig. 2C). Thus, HIV-1 MLOs are constantly evolving and can fuse to larger, spherical compartments. In particular, HIV-1 MLOs undergo to fusion and fission (Fig. 2C, S2B), which is a LLPS-related feature.

Of note, biomolecular condensates follow the characteristics of liquids, thus, they usually contain highly dynamic molecules that exchange both within the condensate and with the surrounding environment (Alberti et al., 2019). To evaluate whether virus-induced CPSF6 clusters present the aforementioned features we evaluated their fluorescence recovery after photobleaching (FRAP). We observed that after the laser irradiation (200 µs/px) the florescence of CPSF6 was rapidly restored (~ 2 minutes), indicating the exchange of fluorescent CPSF6 molecules inside and outside the MLO (Fig. 2D, video 2).

We have also observed that CPSF6 phase separation does not randomly occur in the nuclear space. CPSF6 clusters fully colocalize with the marker of nuclear speckles (NSs), SC35 (Fig.2E), in line with previous studies (Francis et al., 2020; Rensen et al., 2020). We remarked that CPSF6 and SC35 signals mainly occupy the interchromatin space (Fig.2E). NSs are, indeed, storage sites of splicing and other mRNA processing

factors and were firstly defined as interchromatin granules (Spector and Lamond, 2011). However, even if the core of NS excludes the host chromatin, a subset of active genes locate in NS periphery, in the so-called speckle associated domains (SPADs) (Kim et al., 2020; Shopland et al., 2003).

The newly synthesized double-stranded viral DNA separates from HIV-1 MLOs.

To decipher the nuclear location of the newly synthesized ds vDNA we benefited of the HIV-1 ANCHOR DNA tagging system (Fig. S3A)(Blanco-Rodriguez et al., 2020). Once fully reverse transcribed, the HIV-1 genome carrying the bacterial sequence ANCH3 is specifically recognized by OR-GFP protein, which is expressed in the target cells, genetically modified by the lentiviral vector (LV) OR-GFP (Blanco-Rodriguez et al., 2020) (Fig. S3A). The accumulation of OR-GFP, which is a modified version of the bacterial ParB protein (Graham et al., 2014; Sanchez et al., 2015), on the ANCH3 sequence generates bright nuclear signals (Fig. 3A,B, Fig. S3 B,C). OR protein binds exclusively the ds DNA (Saad et al., 2014). We cloned ANCH3 in the nef gene, thus, HIV-1 ANCHOR system exclusively detects the final products of the RT, because the ANCH3 sequence is one of the last sequences to be converted into ds DNA (Fig. S3A). Thus, the system tracks the vDNA forms that will potentially be engaged in the PIC. Unlike previous studies based on viral protein tracking (Burdick et al., 2017; Burdick et al., 2020; Chin et al., 2015; Francis et al., 2020; Francis and Melikyan, 2018; Lelek et al., 2012), we are now able to directly visualize in fixed and live cells individual nuclear vDNA (GFP spots). The high specificity of HIV-1 ANCHOR system to detect the newly synthesized vDNA is shown by the correlation between the nuclear GFP puncta and the MOI (multiplicity of infection) used (Fig. S3B). In addition, the RT inhibitor, NEV, completely prevents the detection of vDNA (Fig. S3B). We also assessed that HIV-1 ANCHOR can detect both vDNAs, episomal and integrated forms. Indeed, this labeling system can reveal intranuclear GFP spots in infected cells treated with an inhibitor of integration, Raltegravir (RAL), or by using an integration defective virus (HIV-1 ANCH3 IN_{D116A}). Results were confirmed by qPCR (Fig. S3C). Importantly, we also observed that HIV-1 ANCHOR is sufficiently sensitive to allow the detection of a single provirus, as shown by the results of HIV integrations (ALU PCR) and of single cell imaging of a selected clone (Fig. S3D).

Intriguingly, when we labelled late reverse transcripts location with respect to the IN foci present in HIV-1 MLOs, we found a complete separation, since their association was extremely rare (Fig. 3A). The HIV-1 IN-vDNA nuclear dynamics represent a long-standing and debated topic. There are, indeed, multiple challenges due to the short-time nature of the event or the technical limitations of vDNA and IN visualization. Thus, to confirm our data we performed live-imaging, asking whether we could pinpoint the dynamic evolution of this separation, coupling the HIV-1 ANCHOR system with the Gag-integrase-Ruby (GIR) virus (generous gift from Edward Campbell) (Dharan et al., 2016; Hulme et al., 2015) (Fig. 3B, video 3,4). The virus is produced using a viral genome carrying ANCH3 sequence and the IN mutated in the catalytic site (HIV-1 ANCH3 IN_{D116A}) together with the GIR plasmid. As consequence, the only functional IN in these viral particles is the IN-Ruby. Performing multiple videos in HeLa cells during a non-synchronized infection (starting from 13.30 h p.i.), we found IN foci colocalizing with the vDNA before their separation (Fig.3B and video 4). We analysed the association of the two signals that rapidly (~ 10 min) separated (Fig. 3B). Since the infection was not synchronized, we had the opportunity to visualize in a single cell different viral dynamics (video 4). Overall, our results suggest that the IN proteins that are part of the HIV PIC are unlikely to be detected by a conventional light microscope, indeed only few IN proteins are part of the PIC (Ballandras-Colas et al., 2017; Hare et al., 2009). The vDNA/IN separation data in fixed and live cells indicated that final products of the RT are released from HIV-1 MLO sites once synthesized, in line with a recent study (Muller et al., 2021). At three days p.i., nearly all double-stranded late reverse transcripts were excluded from HIV-1 MLO cores (Fig. 3C), as also suggested from the separation of the vDNA from the IN puncta (Fig. 3A,B). The majority of the viral IN visible by confocal remain sequestered in CPSF6 clusters (Fig.1A), likely as part of other viruses retained in these organelles.

Next, we investigated the nuclear space distribution of the final products of the RT. We computed the 3D distances of the ds vDNAs from the boundary of the closest NS. We calculated that ds vDNAs locate near NS at a distance ~ 0.57 µm in average (Fig. 3C). Overall, our results show that the vDNAs labelled by HIV-1 ANCHOR are mainly excluded from HIV-1 MLOs.

HIV-1 active proviruses locate outside HIV-1 MLOs.

Taking in consideration that the ds vDNAs are found outside HIV-1 MLO (Fig. 3A,B,C), we wondered about the location of viral transcription sites that allow the viral replication. Thus, we coupled HIV-1 ANCHOR with RNA FISH to co-detect the vDNA and the vRNA. The vDNA/vRNA association analysis highlights the transcription sites of the virus in both differentiated THP-1 cells and primary monocyte-derived macrophages (MDMs) (Fig. 4A). Not all vDNAs were associated to a transcriptional focus, because the episomal forms are less actively transcribed than integrated vDNAs. However, some vDNAs co-localize with bright vRNA spots (RNA FISH), suggesting that these are active proviruses.

Next, we focused on the nuclear location of active proviruses in MDMs infected with HIV-1 GFP reporter virus to monitor viral expression (Fig. 4B,C Fig. S4A). Through the immuno-RNA FISH we were able to co-visualize CPSF6 clusters and HIV-1 incoming genomes or the foci of viral transcription, which, respectively located inside or outside HIV-1 MLOs (Fig. 4B). We observed that at three days p.i., MDMs treated with NEV contain only incoming vRNAs sequestered in CPSF6 clusters (Fig. 4B), similarly to THP-1 cells (Fig. 1B). On the other hand, untreated cells presented a mixed population of foci inside and outside HIV-1 MLOs (Fig. 4B). The percentage of excluded vRNA foci correlates with GFP expression (Pearson's r ~0.63) suggesting that these foci are actively transcribing proviruses (Fig. 4B,C).

Moreover, we found that the mean intensity of the vRNA signal in HIV-1 MLOs (MLOs have been selected for the sphericity >95% (Fig. S4B)) was higher in average in NEV treated cells compared to untreated cells (Fig. 4D), likely due to an ongoing RT process (Fig. 1C). The MLOs-excluded vRNA foci can be also tracked down by coupling HIV-1 ANCHOR (vDNA detection) to immune-RNA FISH (vRNA detection), indicating that the sites of viral transcription locate outside CPSF6 clusters (Fig. S4C). The aforementioned result is supported by the reduction of viral transcripts in infected cells treated with RAL (Fig. S4D). This result is consistent with the notion that episomal forms transcribe much less than proviruses (Dupont et al., 2021).

The immune-RNA FISH highlights both vRNA foci inside and outside the MLO (Fig. 5A). On the contrary, when we applied MCP-MS2 system (kind gift from E. Bertrand) (Tantale et al., 2016), we were able to exclusively visualize vRNAs located outside

HIV-1 MLOs. Upon block of viral integration (RAL), we rarely could detect vRNA foci, due to the low level of transcription of episomal forms (Dupont et al., 2021), while in absence of drug we could highlight several vRNA foci, indicating that these bright spots are active proviruses located outside CPSF6 clusters (Fig. S5A). Thus, MCP-MS2 applied in the context of HIV, exclusively detects viral transcription foci (Fig. 5B, Fig. S5A). Besides, we observed that MCP-GFP is hindered in binding incoming vRNA and it is filtered out by HIV-1 MLOs. In fact, upon NEV treatment no viral RNA species were detected inside CPSF6 clusters (Fig.5B). The specificity of MCP-MS2 in the binding vRNA transcription foci could be due to the steric hindrance from the capsid that shields the vRNA genome (Li et al., 2021; Muller et al., 2021; Zila et al., 2021) or because MLOs can act as selective filters (Alberti et al., 2019). However, further investigations are needed to better characterize this phenomenon. In addition, this approach allows the live tracking of individual proviral transcription foci by coupling it to HIV-1 ANCHOR technology (Fig. S5B). Overall, MCP-MS2 is a valuable tool to study the interplay between active proviruses and the surrounding nuclear landscape. Thus, we used MCP-MS2 system to compute the 3D distances of viral transcription foci from the closest NS boundary. We observed that viral replication sites locate in the NS-surrounding chromatin (avg ~ 0.57 µm) (Fig. 5C). It has been found by genomic approaches that HIV-1 favours integration in speckle associated domains (SPADs)(Francis et al., 2020), known to be active chromatin loci. Now, our study allows to spatially distinguish and visualize individual vRNA transcription foci in single cell. In particular, we were able to appreciate the topological nuclear localization of active proviruses.

The HIV-1 replication occurs in LEDGF-chromatin sites near HIV-1-MLOs in macrophage-like cells.

We explored the nuclear landscape surrounding viral replication hubs using HIV-1 ANCHOR and MCP-MS2 labelling systems. Lens Epithelium-Derived Growth Factor (LEDGF)(Ciuffi et al., 2005), which is a host partner of the viral IN (Cherepanov et al., 2003; Ciuffi et al., 2005; Emiliani et al., 2005; Ferris et al., 2010; Hare et al., 2009; Lelek et al., 2015; Llano et al., 2006; Shun et al., 2008; Shun et al., 2007; Wang et al., 2014), participates to HIV-1 integration sites distribution. We observed that LEDGF forms clusters independently of viral infection in macrophage-like cells (Fig. S6).

LEDGF is located in active chromatin regions because its PWWP domain has been shown to interact with H3K36me3 (Pradeepa et al., 2014; Pradeepa et al., 2012), which is a marker of euchromatin. In particular, this post-translational modification is enriched in HIV-1 integration sites (Ciuffi et al., 2005; Lelek et al., 2015; Vansant et al., 2020; Wang et al., 2009). In this study we found LEDGF to be associated to the proviruses forming a complex visible by imaging (Fig. 6A), dissociated from CPSF6 clusters (Fig. 6A). In average ~64% of vDNA and ~73% of vRNA foci per nucleus were found in complex with LEDGF (Fig. 6A). LEDGF is also known to interact with splicing factors (Singh et al., 2015). This agrees with our data showing vDNA and vRNA localized in average at ~ 0.57 µm from the closest NS (Fig. 3C, 5C). Our data support HIV-1-targeted active chromatin surrounding HIV-1 MLOs. More in detail, the foci of viral transcription locate at less than 1 µm from the closest HIV-1 MLO (CPSF6+SC35), whereas the total vDNAs (episomal or integrated forms) are more distant, in average ~1.8 µm (Fig. 6B).

Overall, our results indicate that HIV-1 MLO-neighboring active chromatin regions, marked by LEDGF and in proximity of NS, favour HIV-1 integration, creating a suitable environment for viral replication.

Discussion

Parasites able to integrate their genome into the host DNA have evolved to target chromatin both to favor the release of new progeny and to optimize their coexistence with the host (Bushman, 2003; Craig and Marszalek, 2002). Even though HIV-1 infection is characterized by the silent persistence of the virus in the host cell, HIV needs to rapidly generate high levels of virions during the acute phase, intuitively explaining the preference of active genes as integration targets (Ciuffi et al., 2005; Di Nunzio et al., 2013; Lelek et al., 2015; Maldarelli, 2016; Schroder et al., 2002).

Thus far, CPSF6 has been described as crucial partner of HIV-1 capsid (Buffone et al., 2018; Lee et al., 2010; Price et al., 2014) and as player in HIV-1 integration site selection (Achuthan et al., 2018; Buffone et al., 2018; Sowd et al., 2016). Here, we provide new insights on the properties of CPSF6 protein clusters induced by the infection, and we unravel their unexpected role in HIV-1 pre-integration steps in non-

dividing cells, known to be an important cellular reservoir (Ganor et al., 2019; Kruize and Kootstra, 2019; Real and Bomsel, 2019; Veenhuis et al., 2021). CPSF6 proteins have been previously shown to cluster in NSs upon viral infection (Francis et al., 2020; Rensen et al., 2020). We observed that CPSF6 proteins form condensates that occupy the interchromatin space (Fig. 2E) and host multiple viral components, at early times post-infection (Fig. 1A-B). These host-viral condensates form even in the absence of reverse transcription (Fig. 1B), implying their relevance in early post-nuclear entry stages. In physiological conditions, multiple viral EdU-labelled DNA copies strongly colocalize with CPSF6 clusters (Francis et al., 2020; Rensen et al., 2020). In this study, we showed that the vDNA observed inside CPSF6 clusters is a newly synthesized vDNA. Indeed, the ChIP of the endogenous CPSF6, followed by real time PCR in infected THP-1 cells (48 h p.i.), shows an abundance of early and intermediate compared to late reverse transcription products, indicating an ongoing reverse transcription process in CPSF6 clusters.

We named these nuclear viral/host niches HIV-induced membraneless organelles “HIV-1 MLOs” and we investigated their liquid-liquid phase separation (LLPS) properties in the cell. CPSF6 contains intrinsically disordered mixed-charge domains which are responsible for the formation of CPSF6 condensates *in vitro* (Greig et al., 2020). We show that these clusters match LLPS properties in the cells, being dynamic and evolving along infection (Fig. 2). Furthermore, the recovery of CPSF6 fluorescent after photobleaching indicates the importance of CPSF6 equilibrium maintenance in these structures (Fig. 2D). CPSF6 phase-separation with viral reverse transcription complexes may be induced as response to the nucleoplasm perturbation by HIV, to find a new protein(s) balance. Of note, CPSF6 plays key biological functions, such as in the mRNA processing. We observed an increase of the amount of this protein upon viral infection (Fig.2A) and this phenomenon could ensure a bimodal role of CPSF6, one for the biology of the host cell and the other for the viral replication.

Our data hinted that HIV-1 MLOs have a key role in pre-integration steps. To characterize the later nuclear stages of the virus, we exploited HIV-1 ANCHOR system, which is the only DNA labelling approach permitting in fixed and live cells to track HIV-1 ds DNA, including proviruses (Fig. S3D, Fig. 4A, Fig. S5A). The final reverse transcription products rarely co-localize with IN foci, leaving HIV-1 MLO (Fig.3 A, B).

Using live imaging, we could pinpoint the budding of newly synthesized ds vDNA from the IN clusters, which occurs within minutes (Fig. 3B, video 4). At three days post infection, in non-dividing cells, the vDNA population is composed of both episomal and proviral forms. We find that the vDNAs are excluded from the MLOs and the majority locates around 0.57 µm from the closest SC35-marked nuclear speckle (Fig. 3C). Likely, HIV exploits the induced CPSF6 clusters to generate pre-integration complexes (PICs), which then will depart from these interchromatin sites (Fig. 3B). Notably, HIV-1 ANCHOR is sensitive enough to enlighten single proviruses (Fig. S3D) and through the coupling with virus-specific RNA smiFISH (Tsanov et al., 2016) it is possible to reveal transcriptionally active proviruses (Fig. 3D). The RNA FISH in primary macrophages displays viral transcription foci excluded from CPSF6 clusters, as previously hinted by the vDNA location. The vRNA foci excluded from MLOs positively correlate with the GFP expression used as viral reporter gene (Fig. 4B,C), indicating that the viral replication occurs outside HIV-1 MLOs, while the vRNA genomes reverse transcribe inside (Fig. 1C).

We finally focused on the nuclear landscape of viral expression, exploiting MCP-MS2 tagged viruses, which mark viral transcription foci only, contrary to the RNA FISH (Fig. 5B and S5A, B). Viral RNA transcription foci locate outside HIV-1 MLOs, but in proximity of NSs (Fig. 5C). LEDGF associates to highly-spliced transcriptional units through its direct interaction with several splicing factors (Singh et al., 2015) and determines HIV-1 integration sites distribution in active chromatin sites (Ciuffi et al., 2005; Ferris et al., 2010; Shun et al., 2007). However, a complex formed by the vDNA or vRNA and LEDGF was never highlighted by fluorescence imaging (Fig.6A). We uncovered that most of the cells present a high percentage of vRNA foci associated to LEDGF (Fig. 6A), highlighting the active nature of HIV-1 targeted domains. Lastly, the vRNA transcription foci are closer to CPSF6 + SC35 condensates compared to the total ds vDNA nuclear forms, suggesting that the HIV-1 MLOs-neighbouring regions are preferred hubs of viral replication (Fig. 6B).

Taken together our results show that CPSF6 phase-separates to speckles prompted by the virus, likely, to usurp functions linked to these nuclear bodies. HIV-induced membraneless organelles host viral complexes and their nuclear reverse transcription,

but once the ds vDNA is synthesized, this moves away proceeding with the infection. The neighboring nuclear speckle-associated environment is a favorable active domain for viral replication since active proviruses locate at less than 1 µm from the closest HIV-1 MLOs (Fig. 6B). Our study supports how new single-cell level approaches are pivotal in the study of functional nuclear dynamics of viruses, to discriminate the cells susceptible to fuel viremia or that concur to viral persistence.

Materials and Methods

Cell lines, primary cells and generation of HIV-1 ANCH3 single-cell clones.

THP-1 (ATCC) are immortalized monocytic cells that once seeded, were differentiated into macrophage-like cells under Phorbol 12-myristate 13-acetate (PMA) treatment (167nM). HEK 293T cells (ATCC) are human embryonic kidney cells used to produce lentiviral vectors and HIV-1. HeLa P4R5 are β-galactosidase reporter cells expressing CD4, CXCR4, CCR5 (Charneau et al., 1994). HeLa MCP-GFP cells stably express MCP-GFP bacterial fusion protein (Tantale et al., 2016). THP-1 cells were cultivated in RPMI 1640 medium supplemented with 10% Fetal Bovine Serum (FBS) and 1% penicillin-streptomycin solution (100 U/mL). HEK293T and HeLa P4R5 cells were cultivated in DMEM medium supplemented with 10% Fetal Bovine Serum (FBS) and 1% penicillin-streptomycin (100 U/mL). Primary monocyte-derived macrophages (MDMs) were obtained by PBMCs buffy coat isolation from healthy donors' blood via EFS (Etablissement Français du Sang, Paris), through density gradient centrifugation with Ficoll 400. The PBMCs were then incubated at 37°C for 2 hours, next, non-adherent cells were washed away, and complete RPMI 1640 medium was supplemented with M-CSF (10 ng/mL). After 3 days, the medium was changed with RPMI without M-CSF and cells were left to differentiate for other 4 days before proceeding with infections.

HIV-1 ANCH3 single-cell clone was generated starting from HeLa P4R5 cells which were infected with HIV-1 ANCH3 (MOI 1). Cells were diluted to 1 cell per well, in 96-well plates. Cell-clone colonies were tested for β-galactosidase expression to check viral infectivity (kit Roche #11758241001). Positive clones were transduced with the lentiviral vector (LV) CMV-OR-GFP for the imaging of HIV-1 ANCH3 provirus. All cells were kept in incubator at 37°C and 5% CO_2.

Plasmids, lentiviral vectors, and viral productions.

HIV-1ΔEnvIN$_{HA}$ΔNef plasmid encodes for the ΔEnvHIV-1 LAI (BRU) viral genome where the integrase (IN) protein is fused to the hemagglutinin (HA) tag (Petit et al., 1999; Petit et al., 2000). HIV-1ΔEnvIN$_{HA}$ΔNef ANCH3 (HIV-1 ANCH3) was obtained through ANCH3 insertion: ANCH3 sequence was cloned by PCR using the template plasmid pANCH3 as we previously described in Blanco et al. (Blanco-Rodriguez et al., 2020). The ANCHOR^{TM} technology and sequences are exclusive property of NeoVirTech (Germier et al., 2017; Mariame et al., 2018). HIV-1ΔEnv IN$_{HA}$(D116A) ΔNef ANCH3 (HIV-1 ANCH3 IN$_{D116A}$) was obtained by insertional mutagenesis using the QuikChange II XL Site-Directed Mutagenesis kit (Agilent #200522), for integrase (IN) mutation at D116. The lentiviral vector plasmid pSICO-CPSF6-mNeonGreen encoding CPSF6 fluorescent fusion protein was purchased by Addgene (#167587). HIV-1ΔEnvIN$_{HA}$ΔNef ANCH3 MS2 plasmid was obtained by inserting the MS2x64 sequence, from pMK123-MS2x64 plasmid, (kindly provided by E. Bertand) (Tantale et al., 2016) in HIV-1ΔEnvIN$_{HA}$ΔNef ANCH3. HIV-1 ΔEnv Δnef IRES GFP plasmid encodes for the ΔEnvHIV-1 NL4.3 GFP viral genome (Rensen et al., 2021). The lentiviral vector plasmids CMV OR-GFP and CMV OR-SANTAKA were obtained by cloning OR-GFP/OR-SANTAKA cassette (plamids from NeoVirTech) in a pTripCMV (ΔU3) plasmid through PCR using restriction site, AgeI and SgrDI.

Lentiviral vectors and HIV-1 viruses were produced by transient transfection of HEK293T cells through calcium chloride coprecipitation. Co-transfection was performed as follows: for lentiviral vectors 10 µg of transfer vector, 10 µg of packaging plasmid (gag-pol-tat-rev) and 2.5 µg of pHCMV-VSV-G envelope plasmid; for VSV-G HIV-1ΔEnv viruses: 10 µg HIV-1ΔEnv plasmid, 2.5 ug of pHCMV-VSV-G plasmid. Lentiviral vectors and viruses for transduction/infection of THP-1 and MDM cells were produced in combination with 3 µg of SIV$_{MAC}$ Vpx (Durand et al., 2013). HIV-1 ANCH3 IN$_{D116A}$ has been also produced in combination with GIR (Gag-IN-Ruby plasmid) (Dharan et al., 2016; Hulme et al., 2015) for IN/vDNA live microscopy. After the collection of the supernatant 48h post-transfection, lentiviral particles were concentrated by ultracentrifugation for 1 h at 22000 rpm at 4°C and stored at −80°C. Lentiviral vectors and viruses were tittered through qPCR in HEK293T cells, 3 days post transduction.

Chromatin Immunoprecipitation with qPCR

Four hundred million of THP-1 cells infected or not with HIV-1 (MOI 5) were fixed with 1% formaldehyde for 15 min and quenched with 0.125 M glycine, then sent to Active Motif Services (Carlsbad, CA) to be processed for ChIP-qPCR. In brief, chromatin was isolated by the addition of lysis buffer, followed by disruption with a Dounce homogenizer. Lysates were sonicated and the DNA sheared to an average length of 300-500 bp. Genomic DNA (Input) was prepared by treating aliquots of chromatin with RNase, proteinase K and heat for de-crosslinking, followed by ethanol precipitation. Pellets were resuspended and the resulting DNA was quantified on a Nanodrop spectrophotometer. Extrapolation to the original chromatin volume allowed quantitation of the total chromatin yield. An aliquot of chromatin (40 µg) was precleared with protein A agarose beads (Invitrogen). Genomic DNA regions of interest were isolated using 4 µg of antibody against CPSF6 (#NBP1-85676). Complexes were washed, eluted from the beads with SDS buffer, and subjected to RNase and proteinase K treatment. Crosslinks were reversed by incubation overnight at 65°C, and ChIP DNA was purified by phenol-chloroform extraction and ethanol precipitation. Quantitative PCR reactions were carried out in triplicate on specific genomic regions using SYBR Green SuperMix (BioRad). The resulting signals were normalized for primer efficiency by carrying out qPCR for each primer pair using Input DNA. Different RT products were amplified using the following primers, early RT products: 5′-GCCTCAATAAAGCTTGCCTTGA-3′ and 5′-TGACTAAAAGGGTCTGAGGGATCT-3′; intermediate RT products: 5′ -CTAGAACGATTCGCAGTTAATCCT-3′ and 5′ -CTAT CCTTTGAT GCACACAATAGAG-3′; late RT products: 5′-TGTGTGCCCGTCTGTTGTGT-3′ and 5′-GAGTCCTGCGTCGAGAGAGC-3’. A group of control genes were also amplified to show the enrichment of HIV-1 specific DNA in the infected condition. De-crosslinked ChIP products were checked by western blot against CPSF6 (same ChIP antibody (#NBP1-85676)), loading 37.5 ng of DNA per sample.

RNA FISH and IMMUNO-RNA FISH

THP-1 cells were seeded on coverslips (12mm #1, ThermoFisher) and differentiated with PMA (167 nM) for 48h. Next, the cells were transduced with OR-GFP LV (MOI 0.5) and then infected with HIV-1 ANCH3 (MOI 20) for 3 days. The medium was always supplemented with PMA. Primary MDMs were seeded before differentiation on coverslips and after 7 days, transduced with OR-GFP LV (MOI 10) and infected with

HIV-1 ANCH3 (MOI 40) for 4 days. The day of fixation the cells were washed with PBS and fixed with 4% PFA for 15 minutes and incubated in 70% ethanol at -20°C at least for one overnight. Primary smiFISH probes have been designed against HIV-1 *pol* transcript and a shared readout sequence for secondary probe alignment. Twenty-four smiFISH probes (Table S1) against HIV pol were designed with Oligostan (Tsanov et al., 2016) and purchased from Integrated DNA Technologies (IDT). Primary probes were pre-hybridized with a secondary FLAP probe conjugated to Cy5 fluorophore (Eurofins) through pairing with the readout sequence. Washes and hybridization were performed with Stellaris Buffers (WASH buffer A, WASH buffer B, Hybridization Buffer; LGC Biosearch Technologies), following the manufacturer protocol. Hybridization with the probe was carried out at 37°C in a dark humid chamber for 5 hours.

For the immuno-RNA FISH THP-1 cells were seeded on coverslips and differentiated with PMA (167 nM) for 48h and then infected with HIV-1 (MOI and time points indicated in figure legends). NEVIRAPINE (NEV) 10 µM or RALTEGRAVIR (RAL) 20 µM were used to block respectively DNA synthesis or integration. Primary MDMs were seeded before differentiation on coverslips and after 7 days infected with HIV-1 GFP reporter virus for 2-3 days. Fixation was carried on in 4% PFA for 15 minutes and then the coverslips where incubated with a blocking/permeabilization solution (PBS-BSA 1%, 2mM Vanadyl ribonucleoside complexes (VRCs) solution (Sigma #94742), TRITON-X 0.3%) for 1 h. Then, the coverslips were incubated with anti-CPSF6 1:400 (#NBP1-85676) in blocking/permeabilization solution for 1h, washed and incubated for 45 min with anti-Rabbit secondary antibody, at room temperature, in the dark, in humid chamber. The coverslips were fixed again in PFA 4% for 10 min. Subsequent RNA FISH and mounting protocol was carried out as mentioned before, but the hybridization with the probes was carried on overnight.

Finally, all the coverslips were stained with Hoechst 33342 1:5000 (Invitrogen #H3570) for 5 minutes and mounted on glass slides (Star Frost) with Prolong Diamond Antifade Mountant (Life Technologies #P36970). Confocal microscopy was carried out with a Zeiss inverted LSM700 microscope, with a 63X objective (Plan Apochromat, oil immersion, NA=1.4).

Epifluorescence and Immunofluorescence of HIV-1 infected cells

The cells were plated on coverslips (12mm #1, ThermoFisher). THP-1 cells were differentiated with PMA (167 nM) for 48h and then infected transduced/infected (MOI and time post-infection indicated in figure legends). For late reverse transcripts or RNA visualization the cells were transduced with OR-GFP LV (MOI 0.5) or MCP-GFP LV (MOI 2) and 48 h later infected with HIV-1 ANCH3 or HIV-1 ANCH3 MS2, respectively. The medium was always supplemented with PMA. For HIV-1 ANCH3 imaging in HeLa P4R5, the cells were transduced with OR-GFP LV (MOI 0.2) and then infected 24 hours later with HIV-1 ANCH3 or HIV-1 IN_{D116A} ANCH3 + NEVIRAPINE (NEV) 10 µM or RALTEGRAVIR (RAL) 20 µM drugs were used to block respectively DNA synthesis or integration. The day of fixation the cells were washed with PBS and fixed with 4% PFA for 15 minutes. For protein staining, cells were treated with glycine 0.15% for 10 min, permeabilized with 0.5% Triton X-100 for 30 min and blocked with 1% bovine serum albumin (BSA) for 30 min. All antibody incubations were carried out at room temperature, in the dark, in humid chamber, 1h with primary antibodies and 45 min with secondary antibodies. Washes between antibody incubations and antibodies dilution were done in 1% BSA. Primary antibodies were diluted as follows: anti-HA 1:500 (Roche #11867423001), anti-CPSF6 1:400 (Novus Biologicals #NBP1-85676), anti-SC35 1:200 (Abcam #ab11826), anti-LEDGF 1:200 (BD Bioscience #611715). Secondary antibodies used were the following: Donkey anti-Rabbit Cy3 1:1000 (Jackson Lab #711-165-152), Goat anti-Rabbit Alexa-488 1:300 (Invitrogen #A32731), Goat anti-Mouse Alexa-647 1:300 (Invitrogen #A21235); Donkey anti-Rat Alexa-488 (Invitrogen # A21208) or Goat anti-Rat Alexa-647 (Invitrogen #A21247) 1:100 for IN-HA. Finally, cells were stained with Hoechst 33342 1:10000 (Invitrogen #H3570) for 5 minutes. Coverslips were mounted on glass slides (Star Frost) with Prolong Diamond Antifade Mountant (Life Technologies #P36970). Confocal microscopy was carried out with a Zeiss LSM700 inverted microscope, with a 63X objective (Plan Apochromat, oil immersion, NA=1.4).

FRAP and time-lapse microscopy

For all time-lapse studies the cells were plated in a polymer-coverslip bottom µ-Dish 35 mm (ibidi #81156) at least 24 hours before 2D or 3D video acquisition. Two million of THP-1 cells were differentiated for 48 h and then transduced with CPSF6 mNeonGreen LV (MOI 0.01) for 3 days. Next, the cells were infected with HIV-1 and the live imaging was performed 24-48 h p.i. For CPSF6 clusters fusion studies CPSF6

mNeonGreen positive cells were imaged every 5 min in 2D with a Biostation IM-Q (Nikon).

For Fluorescence Recovery After Photobleaching (FRAP) experiments, the selected clusters were irradiated for 200µs/pixel with 488 laser and after bleaching the frames were acquired in continuous (90 ms) for 5 minutes through a Ti2E inverted microscope (Nikon), based on a CSU-W1 spinning-disk (Yokogawa), using a 60X objective (Plan Apochromat, oil immersion, NA=1.4).

Experiments of co-live tracking of IN-Ruby (GIR) and viral DNA (OR-GFP) were performed in HeLa P4R5 cells transduced with OR-GFP LV (MOI 0.2). The following day, cells were infected with HIV-1 ANCH3 IN_{D116A} GIR virus (MOI 50). Frames were acquired every minute in 3D (stacks spacing 0.4 µm) with the UltraView VOX inverted microscope (Perkin-Elmer), based on a CSU-X spinning-disk (Yokogawa), and using a 63X objective (Plan Apochromat, oil immersion, NA=1.4).

Imaging Analysis and Statistics

All data were analyzed with GraphPad Prism 9 (GraphPad Software, La Jolla California USA, www.graphpad.com), statistic tests are indicated in figure legends. All images and videos were analysed in Fiji (Schindelin et al., 2012) and Icy software 2.2.1.0 (de Chaumont et al., 2012). In particular, CPSF6 clusters segmentation was performed though HK-Means block in Icy (Dufour et al., 2008) followed by ROI statistics exportation (e.g., Mean Intensity, Volume, Area, Sphericity/Circularity defined as the normalised ratio between the contour and interior of the ROI, expressed as a percentage (100% for a circle or sphere). For the vDNA/vRNA distance form SC35 or HIV-1 MLO the 3D confocal images were processed for multi-channel image splitting, vDNA and SC35 segmentation. The automated 3D segmentation of cell nuclei included a preliminary non-local means denoising step to cope with the strong signal heterogeneity and the segmentation of SC35 was readjusted to low contrast conditions. The 3D boundary-to-boundary distance was computed between each vDNA or vRNA spot and its closest SC35 speckle or the closest HIV-1 MLO (SC35+CPSF6).

Quantitative PCR and primers

For HIV-1 ANCH3 DNA forms quantification in HeLa P4R5 cells, a total DNA of 10^6 infected cells (MOI 30) was extracted at 6 hours post infection for Late Reverse

Transcripts (LRTs) qPCR and 24 hours post infection for 2LTR-circles and ALU-PCR, through QIAmp DNA micro kit (QIAGEN #56304). Real-Time PCR of LRTs was performed to assess DNA synthesis and used to normalize qPCR data on viral input, the reactions were carried on in 20 µL, in iTaqUniversal SYBR Green Supermix (Bio-Rad #1725124) using primers for U3 sequence: U3 FX: 5'-TTCCGCTGGGGACTTTCCAGGG-3', U3 RX: 5'-AGGCTCAGATCTGGTCTAACC-3'. Real-Time PCR of 2LTR-circles was used to asses nuclear import efficiency. Reactions were performed in 20 µL, in Maxima Probe/ROX qPCR Mastermix (ThermoFisher #K0232) using primers for 2LTR-circle junction: 2LTR FX: 5'-AACTAGGGAACCCACTGCTTAAG-3', 2LTR RX: 5′-TCCACAGATCAAGGATATCTTGTC-3′, 2-LTR probe: 5'-(FAM)-ACACTACTTGAAGCACTCAAG-GCAAGCTTT-(TAMRA)-3'. Proviral integration quantification of HeLa P4R5 infected cells and HIV-1 ANCH3 clone was performed through ALU PCR, consisting in a first non-kinetic PCR step in 50 µL using Platinum SuperFi DNA Polymerase kit (ThermoFisher #12351250) for the amplification of ALU-U3 fragments and in a second step of HIV-1 specific qPCR reaction in 20 µL in Maxima Probe/ROX qPCR Mastermix (ThermoFisher #K0232). Primer Alu 166: 5'-TCCCAGCTACTCGGGAGGCTGAGG-3', Alu 2: 5'-GCCTCCCAAAGTGCTGGGATTACAG-3', LambdaU3: 5′-ATGCCACGTAAGCGAAACTTTCCGCTGGGGACTTTCCAGGG-3′ for ALU PCR. Lambda: 5'-ATGCCACGTAAGCGAAACT-3', U5: 5'-CTGACTAAAAGGGTCTGAGG-3', Probe: 5'-(FAM)- TTAAGCCTCAATAAAGCTTGCCTTGAGTGC-(TAMRA) for qPCR (Di Nunzio et al., 2013). In all experiments β-actin detection was used for normalization. β-actin FX: 5'-AACACCCCAGCCATGTACGT-3', β-actin RX: 5-CGGTGAGGATCTTCATGAGGTAGT-3', β-actin probe: (FAM)-CCAGCCAGGTCCAGACGCAGGA-(BHQ1).

Acknowledgements

We wish to thank Marion Louveaux and Dmitry Ershov for image analysis help, Philippe Souque and Selen Ay for experimental help. We thank Fabrizio Mammano, Edouard Bertrand, Florian Mueller, and Edward Campbell for sharing reagents. We gratefully acknowledge the UtechS Photonic BioImaging (Imagopole), C2RT, Institut Pasteur, supported by the French National Research Agency (France BioImaging;

ANR-10–INSB–04; Investments for the Future). We thank the NIH AIDS Reagents program to support us with precious reagents. We thank Addgene for the reagents, Franck Gallardo CEO at the NeoVirTech, ActiveMotif for ChIP help. This work was funded by the ANRS REACTing grant ECTZ88162 with a nominative PhD student fellowship ECTZ88177 for V.S., the Sidaction/FRM grant VIH20170718001, the Pasteur Institute.

Competing financial interests: The authors declare no competing financial interests.

References

Achuthan, V., J.M. Perreira, G.A. Sowd, M. Puray-Chavez, W.M. McDougall, A. Paulucci-Holthauzen, X. Wu, H.J. Fadel, E.M. Poeschla, A.S. Multani, S.H. Hughes, S.G. Sarafianos, A.L. Brass, and A.N. Engelman. 2018. Capsid-CPSF6 Interaction Licenses Nuclear HIV-1 Trafficking to Sites of Viral DNA Integration. *Cell Host Microbe*. 24:392-404 e398.

Alberti, S., A. Gladfelter, and T. Mittag. 2019. Considerations and Challenges in Studying Liquid-Liquid Phase Separation and Biomolecular Condensates. *Cell*. 176:419-434.

Ballandras-Colas, A., D.P. Maskell, E. Serrao, J. Locke, P. Swuec, S.R. Jonsson, A. Kotecha, N.J. Cook, V.E. Pye, I.A. Taylor, V. Andresdottir, A.N. Engelman, A. Costa, and P. Cherepanov. 2017. A supramolecular assembly mediates lentiviral DNA integration. *Science*. 355:93-95.

Banani, S.F., A.M. Rice, W.B. Peeples, Y. Lin, S. Jain, R. Parker, and M.K. Rosen. 2016. Compositional Control of Phase-Separated Cellular Bodies. *Cell*. 166:651-663.

Bejarano, D.A., K. Peng, V. Laketa, K. Borner, K.L. Jost, B. Lucic, B. Glass, M. Lusic, B. Muller, and H.G. Krausslich. 2019. HIV-1 nuclear import in macrophages is regulated by CPSF6-capsid interactions at the nuclear pore complex. *Elife*. 8.

Blanco-Rodriguez, G., and F. Di Nunzio. 2021. The Viral Capsid: A Master Key to Access the Host Nucleus. *Viruses*. 13.

Blanco-Rodriguez, G., A. Gazi, B. Monel, S. Frabetti, V. Scoca, F. Mueller, O. Schwartz, J. Krijnse-Locker, P. Charneau, and F. Di Nunzio. 2020. Remodeling of the Core Leads HIV-1 Preintegration Complex into the Nucleus of Human Lymphocytes. *J Virol*. 94.

Buffone, C., A. Martinez-Lopez, T. Fricke, S. Opp, M. Severgnini, I. Cifola, L. Petiti, S. Frabetti, K. Skorupka, K.K. Zadrozny, B.K. Ganser-Pornillos, O. Pornillos, F. Di Nunzio, and F. Diaz-Griffero. 2018. Nup153 Unlocks the Nuclear Pore Complex for HIV-1 Nuclear Translocation in Nondividing Cells. *J Virol*. 92.

Burdick, R.C., K.A. Delviks-Frankenberry, J. Chen, S.K. Janaka, J. Sastri, W.S. Hu, and V.K. Pathak. 2017. Dynamics and regulation of nuclear import and nuclear movements of HIV-1 complexes. *PLoS Pathog*. 13:e1006570.

Burdick, R.C., C. Li, M. Munshi, J.M.O. Rawson, K. Nagashima, W.S. Hu, and V.K. Pathak. 2020. HIV-1 uncoats in the nucleus near sites of integration. *Proc Natl Acad Sci U S A*. 117:5486-5493.

Bushman, F.D. 2003. Targeting survival: integration site selection by retroviruses and LTR-retrotransposons. *Cell*. 115:135-138.

Campbell, E.M., and T.J. Hope. 2015. HIV-1 capsid: the multifaceted key player in HIV-1 infection. *Nat Rev Microbiol*. 13:471-483.

Charneau, P., G. Mirambeau, P. Roux, S. Paulous, H. Buc, and F. Clavel. 1994. HIV-1 reverse transcription. A termination step at the center of the genome. *J Mol Biol*. 241:651-662.

675 Chaudhuri, E., S. Dash, M. Balasubramaniam, A. Padron, J. Holland, G.A. Sowd, F. Villalta, A.N.
676 Engelman, J. Pandhare, and C. Dash. 2020. The HIV-1 capsid-binding host factor CPSF6 is post-
677 transcriptionally regulated by the cellular microRNA miR-125b. *J Biol Chem*. 295:5081-5094.
678 Cherepanov, P., G. Maertens, P. Proost, B. Devreese, J. Van Beeumen, Y. Engelborghs, E. De Clercq,
679 and Z. Debyser. 2003. HIV-1 integrase forms stable tetramers and associates with LEDGF/p75
680 protein in human cells. *J Biol Chem*. 278:372-381.
681 Chin, C.R., J.M. Perreira, G. Savidis, J.M. Portmann, A.M. Aker, E.M. Feeley, M.C. Smith, and A.L. Brass.
682 2015. Direct Visualization of HIV-1 Replication Intermediates Shows that Capsid and CPSF6
683 Modulate HIV-1 Intra-nuclear Invasion and Integration. *Cell Rep*. 13:1717-1731.
684 Ciuffi, A., M. Llano, E. Poeschla, C. Hoffmann, J. Leipzig, P. Shinn, J.R. Ecker, and F. Bushman. 2005. A
685 role for LEDGF/p75 in targeting HIV DNA integration. *Nat Med*. 11:1287-1289.
686 Craig, E.A., and J. Marszalek. 2002. A specialized mitochondrial molecular chaperone system: a role in
687 formation of Fe/S centers. *Cell Mol Life Sci*. 59:1658-1665.
688 de Chaumont, F., S. Dallongeville, N. Chenouard, N. Herve, S. Pop, T. Provoost, V. Meas-Yedid, P.
689 Pankajakshan, T. Lecomte, Y. Le Montagner, T. Lagache, A. Dufour, and J.C. Olivo-Marin. 2012.
690 Icy: an open bioimage informatics platform for extended reproducible research. *Nat Methods*.
691 9:690-696.
692 Dharan, A., N. Bachmann, S. Talley, V. Zwikelmaier, and E.M. Campbell. 2020. Nuclear pore blockade
693 reveals that HIV-1 completes reverse transcription and uncoating in the nucleus. *Nat*
694 *Microbiol*. 5:1088-1095.
695 Dharan, A., S. Talley, A. Tripathi, J.I. Mamede, M. Majetschak, T.J. Hope, and E.M. Campbell. 2016.
696 KIF5B and Nup358 Cooperatively Mediate the Nuclear Import of HIV-1 during Infection. *PLoS*
697 *Pathog*. 12:e1005700.
698 Di Nunzio, F. 2013. New insights in the role of nucleoporins: a bridge leading to concerted steps from
699 HIV-1 nuclear entry until integration. *Virus Res*. 178:187-196.
700 Di Nunzio, F., T. Fricke, A. Miccio, J.C. Valle-Casuso, P. Perez, P. Souque, E. Rizzi, M. Severgnini, F.
701 Mavilio, P. Charneau, and F. Diaz-Griffero. 2013. Nup153 and Nup98 bind the HIV-1 core and
702 contribute to the early steps of HIV-1 replication. *Virology*. 440:8-18.
703 Dufour, A., V. Meas-Yedid, A. Grassart, and J. Olivo-Marin. 2008. Automated quantification of cell
704 endocytosis using active contours and wavelets. *In* 2008 19th International Conference on
705 Pattern Recognition. 1-4.
706 Dupont, L., S. Bloor, J.C. Williamson, S.M. Cuesta, R. Shah, A. Teixeira-Silva, A. Naamati, E.J.D.
707 Greenwood, S.G. Sarafianos, N.J. Matheson, and P.J. Lehner. 2021. The SMC5/6 complex
708 compacts and silences unintegrated HIV-1 DNA and is antagonized by Vpr. *Cell Host Microbe*.
709 29:792-805 e796.
710 Durand, S., X.N. Nguyen, J. Turpin, S. Cordeil, N. Nazaret, S. Croze, R. Mahieux, J. Lachuer, C. Legras-
711 Lachuer, and A. Cimarelli. 2013. Tailored HIV-1 vectors for genetic modification of primary
712 human dendritic cells and monocytes. *J Virol*. 87:234-242.
713 Emiliani, S., A. Mousnier, K. Busschots, M. Maroun, B. Van Maele, D. Tempe, L. Vandekerckhove, F.
714 Moisant, L. Ben-Slama, M. Witvrouw, F. Christ, J.C. Rain, C. Dargemont, Z. Debyser, and R.
715 Benarous. 2005. Integrase mutants defective for interaction with LEDGF/p75 are impaired in
716 chromosome tethering and HIV-1 replication. *J Biol Chem*. 280:25517-25523.
717 Fare, C.M., A. Villani, L.E. Drake, and J. Shorter. 2021. Higher-order organization of biomolecular
718 condensates. *Open Biol*. 11:210137.
719 Farnet, C.M., and W.A. Haseltine. 1991. Determination of viral proteins present in the human
720 immunodeficiency virus type 1 preintegration complex. *J Virol*. 65:1910-1915.
721 Ferris, A.L., X. Wu, C.M. Hughes, C. Stewart, S.J. Smith, T.A. Milne, G.G. Wang, M.C. Shun, C.D. Allis, A.
722 Engelman, and S.H. Hughes. 2010. Lens epithelium-derived growth factor fusion proteins
723 redirect HIV-1 DNA integration. *Proc Natl Acad Sci U S A*. 107:3135-3140.
724 Francis, A.C., M. Marin, P.K. Singh, V. Achuthan, M.J. Prellberg, K. Palermino-Rowland, S. Lan, P.R.
725 Tedbury, S.G. Sarafianos, A.N. Engelman, and G.B. Melikyan. 2020. HIV-1 replication

complexes accumulate in nuclear speckles and integrate into speckle-associated genomic domains. *Nat Commun*. 11:3505.

Francis, A.C., and G.B. Melikyan. 2018. Single HIV-1 Imaging Reveals Progression of Infection through CA-Dependent Steps of Docking at the Nuclear Pore, Uncoating, and Nuclear Transport. *Cell Host Microbe*. 23:536-548 e536.

Ganor, Y., F. Real, A. Sennepin, C.A. Dutertre, L. Prevedel, L. Xu, D. Tudor, B. Charmeteau, A. Couedel-Courteille, S. Marion, A.R. Zenak, J.P. Jourdain, Z. Zhou, A. Schmitt, C. Capron, E.A. Eugenin, R. Cheynier, M. Revol, S. Cristofari, A. Hosmalin, and M. Bomsel. 2019. HIV-1 reservoirs in urethral macrophages of patients under suppressive antiretroviral therapy. *Nat Microbiol*. 4:633-644.

Germier, T., S. Kocanova, N. Walther, A. Bancaud, H.A. Shaban, H. Sellou, A.Z. Politi, J. Ellenberg, F. Gallardo, and K. Bystricky. 2017. Real-Time Imaging of a Single Gene Reveals Transcription-Initiated Local Confinement. *Biophys J*. 113:1383-1394.

Graham, T.G., X. Wang, D. Song, C.M. Etson, A.M. van Oijen, D.Z. Rudner, and J.J. Loparo. 2014. ParB spreading requires DNA bridging. *Genes Dev*. 28:1228-1238.

Greig, J.A., T.A. Nguyen, M. Lee, A.S. Holehouse, A.E. Posey, R.V. Pappu, and G. Jedd. 2020. Arginine-Enriched Mixed-Charge Domains Provide Cohesion for Nuclear Speckle Condensation. *Mol Cell*. 77:1237-1250 e1234.

Hare, S., F. Di Nunzio, A. Labeja, J. Wang, A. Engelman, and P. Cherepanov. 2009. Structural basis for functional tetramerization of lentiviral integrase. *PLoS Pathog*. 5:e1000515.

Hulme, A.E., Z. Kelley, D. Foley, and T.J. Hope. 2015. Complementary Assays Reveal a Low Level of CA Associated with Viral Complexes in the Nuclei of HIV-1-Infected Cells. *J Virol*. 89:5350-5361.

Kim, J., N.C. Venkata, G.A. Hernandez Gonzalez, N. Khanna, and A.S. Belmont. 2020. Gene expression amplification by nuclear speckle association. *J Cell Biol*. 219.

Kruize, Z., and N.A. Kootstra. 2019. The Role of Macrophages in HIV-1 Persistence and Pathogenesis. *Front Microbiol*. 10:2828.

Lee, K., Z. Ambrose, T.D. Martin, I. Oztop, A. Mulky, J.G. Julias, N. Vandegraaff, J.G. Baumann, R. Wang, W. Yuen, T. Takemura, K. Shelton, I. Taniuchi, Y. Li, J. Sodroski, D.R. Littman, J.M. Coffin, S.H. Hughes, D. Unutmaz, A. Engelman, and V.N. KewalRamani. 2010. Flexible use of nuclear import pathways by HIV-1. *Cell Host Microbe*. 7:221-233.

Lelek, M., N. Casartelli, D. Pellin, E. Rizzi, P. Souque, M. Severgnini, C. Di Serio, T. Fricke, F. Diaz-Griffero, C. Zimmer, P. Charneau, and F. Di Nunzio. 2015. Chromatin organization at the nuclear pore favours HIV replication. *Nat Commun*. 6:6483.

Lelek, M., F. Di Nunzio, R. Henriques, P. Charneau, N. Arhel, and C. Zimmer. 2012. Superresolution imaging of HIV in infected cells with FlAsH-PALM. *Proc Natl Acad Sci U S A*. 109:8564-8569.

Li, C., R.C. Burdick, K. Nagashima, W.S. Hu, and V.K. Pathak. 2021. HIV-1 cores retain their integrity until minutes before uncoating in the nucleus. *Proc Natl Acad Sci U S A*. 118.

Li, P., S. Banjade, H.C. Cheng, S. Kim, B. Chen, L. Guo, M. Llaguno, J.V. Hollingsworth, D.S. King, S.F. Banani, P.S. Russo, Q.X. Jiang, B.T. Nixon, and M.K. Rosen. 2012. Phase transitions in the assembly of multivalent signalling proteins. *Nature*. 483:336-340.

Liu, R., F.R. Simonetti, and Y.C. Ho. 2020. The forces driving clonal expansion of the HIV-1 latent reservoir. *Virol J*. 17:4.

Llano, M., D.T. Saenz, A. Meehan, P. Wongthida, M. Peretz, W.H. Walker, W. Teo, and E.M. Poeschla. 2006. An essential role for LEDGF/p75 in HIV integration. *Science*. 314:461-464.

Maldarelli, F. 2016. The role of HIV integration in viral persistence: no more whistling past the proviral graveyard. *J Clin Invest*. 126:438-447.

Mariame, B., S. Kappler-Gratias, M. Kappler, S. Balor, F. Gallardo, and K. Bystricky. 2018. Real-Time Visualization and Quantification of Human Cytomegalovirus Replication in Living Cells Using the ANCHOR DNA Labeling Technology. *J Virol*. 92.

Muller, T.G., V. Zila, K. Peters, S. Schifferdecker, M. Stanic, B. Lucic, V. Laketa, M. Lusic, B. Muller, and H.G. Krausslich. 2021. HIV-1 uncoating by release of viral cDNA from capsid-like structures in the nucleus of infected cells. *Elife*. 10.

Olson, A., B. Basukala, W.W. Wong, and A.J. Henderson. 2019. Targeting HIV-1 proviral transcription. *Curr Opin Virol*. 38:89-96.

Petit, C., O. Schwartz, and F. Mammano. 1999. Oligomerization within virions and subcellular localization of human immunodeficiency virus type 1 integrase. *J Virol*. 73:5079-5088.

Petit, C., O. Schwartz, and F. Mammano. 2000. The karyophilic properties of human immunodeficiency virus type 1 integrase are not required for nuclear import of proviral DNA. *J Virol*. 74:7119-7126.

Pradeepa, M.M., G.R. Grimes, G.C. Taylor, H.G. Sutherland, and W.A. Bickmore. 2014. Psip1/Ledgf p75 restrains Hox gene expression by recruiting both trithorax and polycomb group proteins. *Nucleic Acids Res*. 42:9021-9032.

Pradeepa, M.M., H.G. Sutherland, J. Ule, G.R. Grimes, and W.A. Bickmore. 2012. Psip1/Ledgf p52 binds methylated histone H3K36 and splicing factors and contributes to the regulation of alternative splicing. *PLoS Genet*. 8:e1002717.

Price, A.J., D.A. Jacques, W.A. McEwan, A.J. Fletcher, S. Essig, J.W. Chin, U.D. Halambage, C. Aiken, and L.C. James. 2014. Host cofactors and pharmacologic ligands share an essential interface in HIV-1 capsid that is lost upon disassembly. *PLoS Pathog*. 10:e1004459.

Real, F., and M. Bomsel. 2019. [HIV infection of the genital mucosa in real time]. *Med Sci (Paris)*. 35:209-212.

Rensen, E., F. Mueller, V. Scoca, J.J. Parmar, P. Souque, C. Zimmer, and F. Di Nunzio. 2020. Clustering and reverse transcription of HIV-1 genomes in nuclear niches of macrophages. *EMBO J*:e105247.

Rensen, E., F. Mueller, V. Scoca, J.J. Parmar, P. Souque, C. Zimmer, and F. Di Nunzio. 2021. Clustering and reverse transcription of HIV-1 genomes in nuclear niches of macrophages. *EMBO J*. 40:e105247.

Saad, H., F. Gallardo, M. Dalvai, N. Tanguy-le-Gac, D. Lane, and K. Bystricky. 2014. DNA dynamics during early double-strand break processing revealed by non-intrusive imaging of living cells. *PLoS Genet*. 10:e1004187.

Sanchez, A., D.I. Cattoni, J.C. Walter, J. Rech, A. Parmeggiani, M. Nollmann, and J.Y. Bouet. 2015. Stochastic Self-Assembly of ParB Proteins Builds the Bacterial DNA Segregation Apparatus. *Cell Syst*. 1:163-173.

Schindelin, J., I. Arganda-Carreras, E. Frise, V. Kaynig, M. Longair, T. Pietzsch, S. Preibisch, C. Rueden, S. Saalfeld, B. Schmid, J.Y. Tinevez, D.J. White, V. Hartenstein, K. Eliceiri, P. Tomancak, and A. Cardona. 2012. Fiji: an open-source platform for biological-image analysis. *Nat Methods*. 9:676-682.

Schroder, A.R., P. Shinn, H. Chen, C. Berry, J.R. Ecker, and F. Bushman. 2002. HIV-1 integration in the human genome favors active genes and local hotspots. *Cell*. 110:521-529.

Scoca, V., and F. Di Nunzio. 2021. The HIV-1 Capsid: From Structural Component to Key Factor for Host Nuclear Invasion. *Viruses*. 13.

Selyutina, A., M. Persaud, K. Lee, V. KewalRamani, and F. Diaz-Griffero. 2020. Nuclear Import of the HIV-1 Core Precedes Reverse Transcription and Uncoating. *Cell Rep*. 32:108201.

Sharkey, M., D.Z. Babic, T. Greenough, R. Gulick, D.R. Kuritzkes, and M. Stevenson. 2011. Episomal viral cDNAs identify a reservoir that fuels viral rebound after treatment interruption and that contributes to treatment failure. *PLoS Pathog*. 7:e1001303.

Sharkey, M.E., I. Teo, T. Greenough, N. Sharova, K. Luzuriaga, J.L. Sullivan, R.P. Bucy, L.G. Kostrikis, A. Haase, C. Veryard, R.E. Davaro, S.H. Cheeseman, J.S. Daly, C. Bova, R.T. Ellison, 3rd, B. Mady, K.K. Lai, G. Moyle, M. Nelson, B. Gazzard, S. Shaunak, and M. Stevenson. 2000. Persistence of episomal HIV-1 infection intermediates in patients on highly active anti-retroviral therapy. *Nat Med*. 6:76-81.

Shopland, L.S., C.V. Johnson, M. Byron, J. McNeil, and J.B. Lawrence. 2003. Clustering of multiple specific genes and gene-rich R-bands around SC-35 domains: evidence for local euchromatic neighborhoods. *J Cell Biol*. 162:981-990.

Shun, M.C., Y. Botbol, X. Li, F. Di Nunzio, J.E. Daigle, N. Yan, J. Lieberman, M. Lavigne, and A. Engelman. 2008. Identification and characterization of PWWP domain residues critical for LEDGF/p75 chromatin binding and human immunodeficiency virus type 1 infectivity. *J Virol*. 82:11555-11567.

Shun, M.C., N.K. Raghavendra, N. Vandegraaff, J.E. Daigle, S. Hughes, P. Kellam, P. Cherepanov, and A. Engelman. 2007. LEDGF/p75 functions downstream from preintegration complex formation to effect gene-specific HIV-1 integration. *Genes Dev*. 21:1767-1778.

Singh, P.K., M.R. Plumb, A.L. Ferris, J.R. Iben, X. Wu, H.J. Fadel, B.T. Luke, C. Esnault, E.M. Poeschla, S.H. Hughes, M. Kvaratskhelia, and H.L. Levin. 2015. LEDGF/p75 interacts with mRNA splicing factors and targets HIV-1 integration to highly spliced genes. *Genes Dev*. 29:2287-2297.

Sowd, G.A., E. Serrao, H. Wang, W. Wang, H.J. Fadel, E.M. Poeschla, and A.N. Engelman. 2016. A critical role for alternative polyadenylation factor CPSF6 in targeting HIV-1 integration to transcriptionally active chromatin. *Proc Natl Acad Sci U S A*. 113:E1054-1063.

Spector, D.L., and A.I. Lamond. 2011. Nuclear speckles. *Cold Spring Harb Perspect Biol*. 3.

Strom, A.R., and C.P. Brangwynne. 2019. The liquid nucleome - phase transitions in the nucleus at a glance. *J Cell Sci*. 132.

Suzuki, Y., and R. Craigie. 2007. The road to chromatin - nuclear entry of retroviruses. *Nat Rev Microbiol*. 5:187-196.

Tantale, K., F. Mueller, A. Kozulic-Pirher, A. Lesne, J.M. Victor, M.C. Robert, S. Capozi, R. Chouaib, V. Backer, J. Mateos-Langerak, X. Darzacq, C. Zimmer, E. Basyuk, and E. Bertrand. 2016. A single-molecule view of transcription reveals convoys of RNA polymerases and multi-scale bursting. *Nat Commun*. 7:12248.

Tsanov, N., A. Samacoits, R. Chouaib, A.M. Traboulsi, T. Gostan, C. Weber, C. Zimmer, K. Zibara, T. Walter, M. Peter, E. Bertrand, and F. Mueller. 2016. smiFISH and FISH-quant - a flexible single RNA detection approach with super-resolution capability. *Nucleic Acids Res*. 44:e165.

Vansant, G., H.C. Chen, E. Zorita, K. Trejbalova, D. Miklik, G. Filion, and Z. Debyser. 2020. The chromatin landscape at the HIV-1 provirus integration site determines viral expression. *Nucleic Acids Res*.

Veenhuis, R.T., C.M. Abreu, E.N. Shirk, L. Gama, and J.E. Clements. 2021. HIV replication and latency in monocytes and macrophages. *Semin Immunol*. 51:101472.

Wang, G.P., B.L. Levine, G.K. Binder, C.C. Berry, N. Malani, G. McGarrity, P. Tebas, C.H. June, and F.D. Bushman. 2009. Analysis of lentiviral vector integration in HIV+ study subjects receiving autologous infusions of gene modified CD4+ T cells. *Mol Ther*. 17:844-850.

Wang, H., M.C. Shun, X. Li, F. Di Nunzio, S. Hare, P. Cherepanov, and A. Engelman. 2014. Efficient Transduction of LEDGF/p75 Mutant Cells by Gain-of-Function HIV-1 Integrase Mutant Viruses. *Mol Ther Methods Clin Dev*. 1.

Zila, V., E. Margiotta, B. Turonova, T.G. Muller, C.E. Zimmerli, S. Mattei, M. Allegretti, K. Borner, J. Rada, B. Muller, M. Lusic, H.G. Krausslich, and M. Beck. 2021. Cone-shaped HIV-1 capsids are transported through intact nuclear pores. *Cell*. 184:1032-1046 e1018.

FIGURE LEGENDS

Figure 1. CPSF6 clusters host HIV-1 viral complexes and are hubs of nuclear reverse transcription. A) Confocal microscopy image of HIV-1 infected THP-1 cells (MOI 10, 30h p.i.), compared to uninfected cells. The graph shows the percentages of IN associated to CPSF6, per nucleus (40 cells, 132 IN foci) ± SD. **B)** Confocal

microscopy images of Immuno-RNA FISH in infected THP-1 (MOI 20, 2 days p.i.) treated or not with NEV (10 µM). The graph shows the percentages of vRNA foci associated to CPSF6 per cells, per condition (cells: 56 (-NEV), 34 (+NEV), vRNA: 151 (-NEV), 61 (+NEV)) ± SD. Unpaired t test, **=p ≤ 0.01. **C)** Chromatin Immunoprecipitation of endogenous CPSF6 coupled to real-time PCR of THP-1 cells infected with HIV-1 (MOI 5), 2 days p.i. Different reverse transcription (RT) products were amplified normalized on the input ± SD. One-way ANOVA followed by Tukey's multiple comparison test, *=p ≤ 0.05, **=p ≤ 0.01, ****=p ≤ 0.0001. On the right, Western blot of CPSF6 of ChIP products in infected cells compared to the input. Scale bar: 5 µm.

Figure 2. Phase separation properties of HIV-1 MLOs.

A) Confocal microscopy images of THP-1 cells infected with HIV-1 (MOI 5, 24 h p.i.), compared to uninfected cells. On the right, mean intensity of CPSF6 per nucleus ± SD (n cells = 49, 55). Unpaired t test, ****=p ≤ 0.0001. **B)** Confocal microscopy images of THP-1 cells infected with HIV-1 (MOI 5) + NEV (10 µM) comparing 24h and 72 h p.i. On the right, box plots of the volume (median: ~ 0.19 vs ~ 0.37 μm^3) and sphericity of CPSF6 clusters (n = 125, 95). Unpaired t test, ****=p ≤ 0.0001, ns = not-significant. 3D analysis. **C)** Frames extracted from a 10 hours-time-lapse microscopy in 2D (video 1) of THP-1 cells expressing CPSF6 mNeonGreen infected with HIV-1 (MOI 10). The graph shows the circularity (normalised ratio between the contour and interior expressed as a percentage) along the memebraneless organelles fusion-fission event. Representative of 6 independent experiments. **D)** Frames extracted form a Fluorescence Recovery After Photobleaching (FRAP) time-lapse (video 2) in THP-1 cells expressing CPSF6 mNeonGreen infected with HIV-1 (MOI 10, 3 days p.i.). Representative of 3 independent experiments. The graph shows the Log_{10} of the mean intensity of the bleached cluster compared to an unbleached cluster in the same cell. **E)** Confocal microscopy image of THP-1 cell infected with HIV-1 (MOI 10, 3 days p.i.). The graph on the left shows the intensity profile of Hoechst, CPSF6, SC35 signal along the segment crossing the MLO (yellow). On the right, the percentage of CPSF6 colocalizing with SC35 per nucleus ± SD, 3D analysis. Scale bar: 5 µm.

Figure 3. Complete reverse transcribed products are released from HIV-1 MLOs.

A) Confocal images of THP-1 cell expressing OR-GFP, infected with HIV-1 ANCH3 (MOI 10, 30h p.i.) compared to uninfected cell. The graph shows the percentages of vDNAs associated to IN, per nucleus (13 cells, 100 vDNAs) ± SD, 3D analysis. **B)** Representative cropped frames from a time-lapse microscopy (video 4) of vDNA (green) and IN (red) dynamics in HeLa P4R5 cells (HIV-1 ANCH3 IN_{D116A} GIR, 18 h p.i.). Pearson's correlation per 2D time frame is shown below. Scale bar: 1 µm. **C)** Confocal image of THP-1 cells expressing OR-GFP infected with HIV-1 ANCH3 (MOI 10, 3 days p.i.). On the bottom, the graphs display: the percentage of vDNA associated to CPSF6 clusters, per nucleus (17 cells, 146 vDNAs) and the distance of each vDNA from the closest SC35-marked nuclear speckle border (7 cells, 83 vDNAs). ± SD, 3D analysis. Scale bar: 5 µm

Figure 4. Active proviruses are excluded from HIV-1 MLOs.

A) Confocal images of THP-1 and primary macrophages (MDMs) cells expressing OR-GFP, infected with HIV-1 ANCH3 (THP-1: MOI 20, 3 days p.i., MDMs: MOI 40, 4 days p.i) 3D analysis. **B)** Confocal images of Immuno-RNA FISH in primary MDMs infected with HIV-1 GFP (MOI 20) ± NEV (10 µM), 2-3 days p.i. The scatter plots show the GFP intensity ± SD per cell and the percentage of vRNA outside CPSF6 clusters ± SD per nucleus (cells: 22 (-NEV), 20 (+NEV); vRNAs: 268 (-NEV), 66 (+NEV)); unpaired t test, ****=p ≤ 0.0001. **C)** Correlation in infected cells (Pearson's r coefficient, **=p ≤ 0.01) of GFP intensity and % of vRNA foci exclusion from CPSF6 clusters (22 cells). **D)** vRNA intensity ± SD per CPSF6 clusters in ± NEV conditions; unpaired t test, **=p ≤ 0.01. The analyses were performed in 3D. Scale bar: 5 µm.

Figure 5. MCP-MS2 RNA labelling detects transcription foci only.

A) Confocal images of Immuno-RNA FISH in THP-1 cells infected with HIV-1 ± NEV (10 µM), (MOI 20, 3 days p.i.). The graph shows the number of vRNA per nucleus, the table shows the amount of vRNA inside or outside CPSF6 clusters (n = 70 cells (-NEV), 68 cells (+NEV)). **B)** Confocal images of THP-1 cells expressing MCP-GFP infected with HIV-1 ANCH3 MS2 ± NEV (10µM), (MOI 2.5, 3 days p.i.). The graph shows the number of vRNA per nucleus, the table shows the amount of vRNA inside or outside CPSF6 clusters (n = 40 cells (-NEV), 44 cells (+NEV)). **C)** Confocal images of THP-1 cell expressing MCP-GFP infected with HIV-1 ANCH3 MS2 (MOI 2.5, 3 days p.i.). The

graph shows the distance of each RNA focus from the closest SC35-marked nuclear speckle border (31 vRNAs, 8 cells) ± SD, 3D analysis. Scale bar: 5 µm, inset: 1 µm.

Figure 6. HIV-1 active proviruses locate in LEDGF-marked chromatin neighboring HIV-1 MLOs. A) Confocal image of THP-1 cells expressing OR-GFP infected with HIV-1 ANCH3 (MOI 10, 3 days p.i.) and expressing MCP-GFP infected with HIV-1 ANCH3 MS2 (MOI 2.5, 3 days p.i.). The plot shows the percentage of CPSF6 clusters associated with LEDGF per nucleus (38 cells, 161 CPSF6) ± SD and the percentage of vDNA or vRNA associated to LEDGF cluster per nucleus ± SD. **B)** Scatter plot with bars indicating the distance of vDNA or vRNA from the border of the closest (SC35+CPSF6) MLO ± SD (n = 75 vDNAs, 7 cells; 34 vRNAs, 8 cells). Unpaired t test, **=p ≤ 0.01. Scale bar: 5 µm, inset: 1 µm.

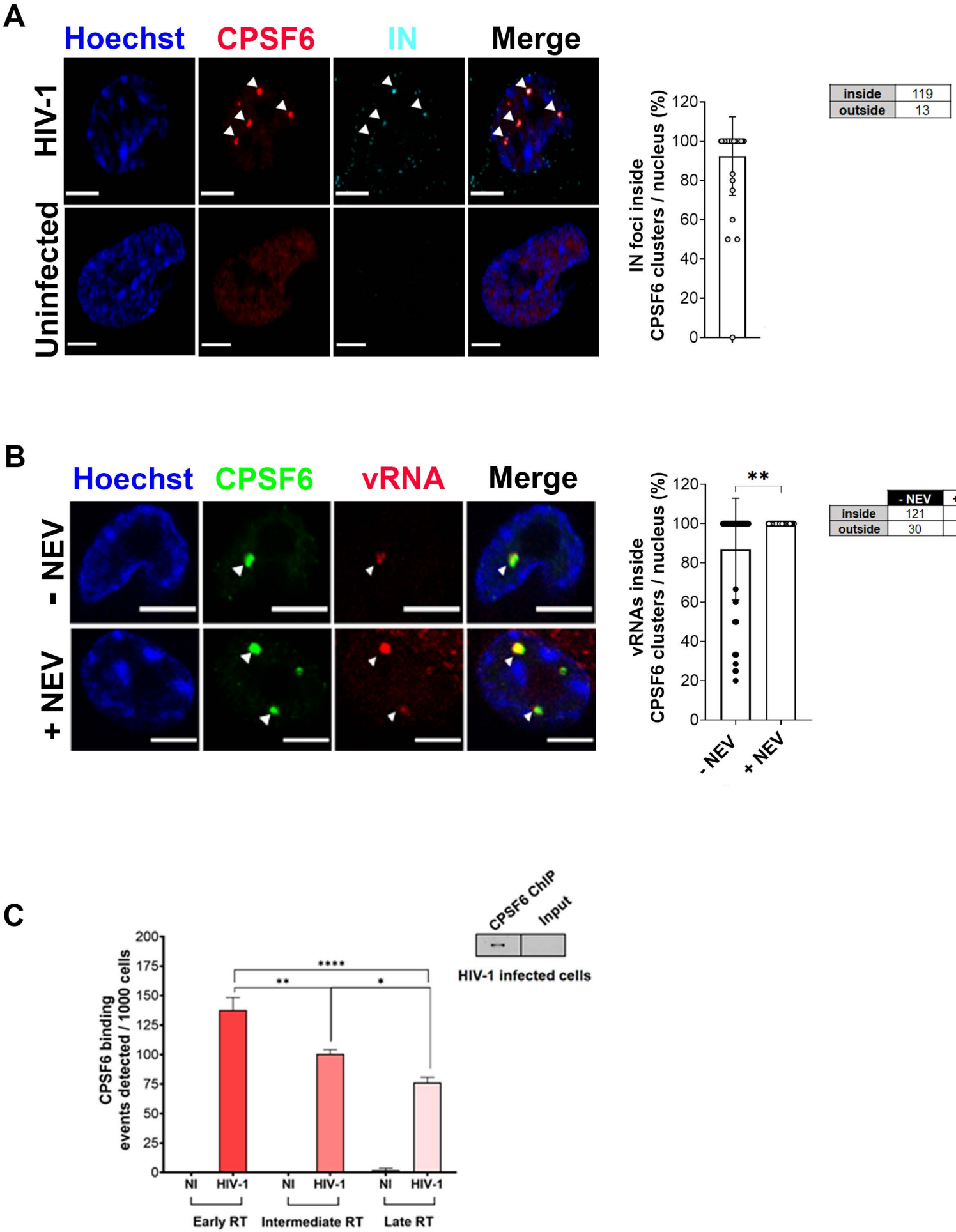
A
Hoechst
CPSF6
IN
Merge
HIV-1
Uninfected
IN foci inside
CPSF6 clusters / nucleus (%)
120
100
80
60
40
20
0
inside 119
outside 13
B
Hoechst
CPSF6
vRNA
Merge
- NEV
+ NEV
vRNAs inside
CPSF6 clusters / nucleus (%)
**
- NEV
+ NEV
inside 121 60
outside 30 0
C
CPSF6 ChIP
Input
HIV-1 infected cells
CPSF6 binding
events detected / 1000 cells
200
175
150
125
100
75
50
25
0
****
**
*
NI
HIV-1
Early RT
Intermediate RT
Late RT

Figure 1

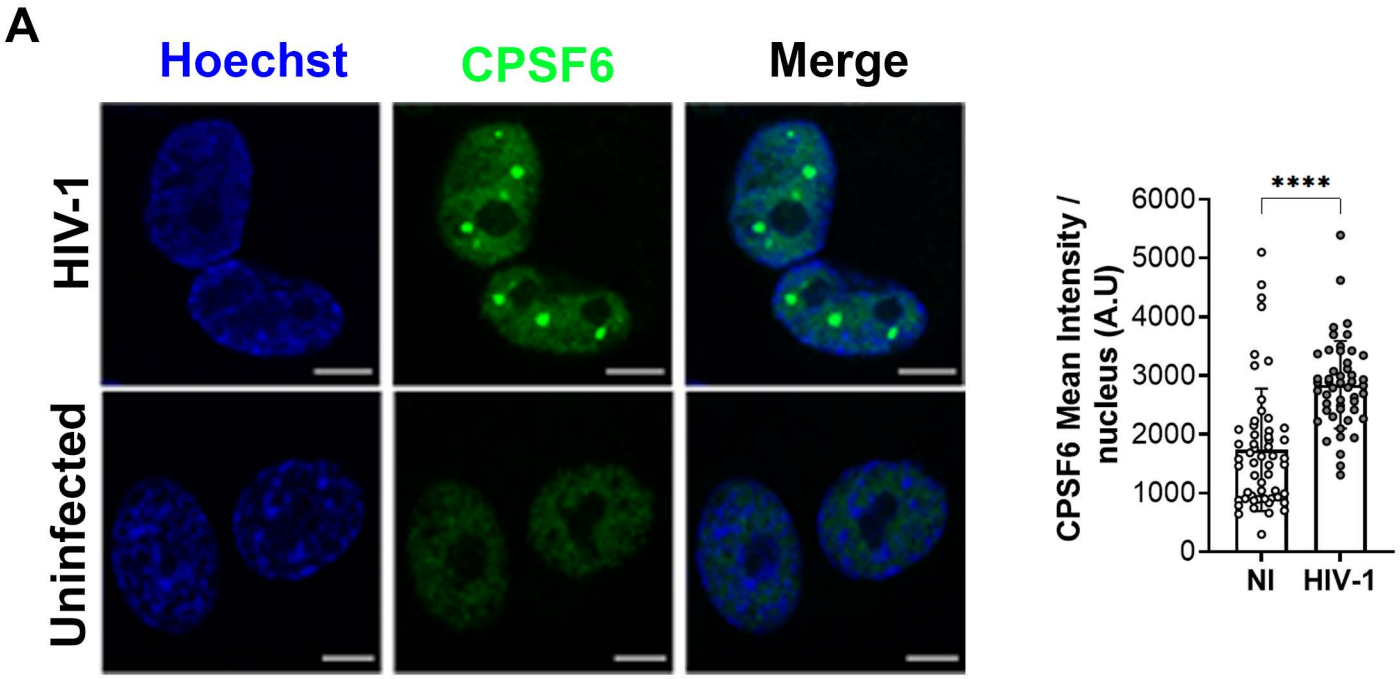

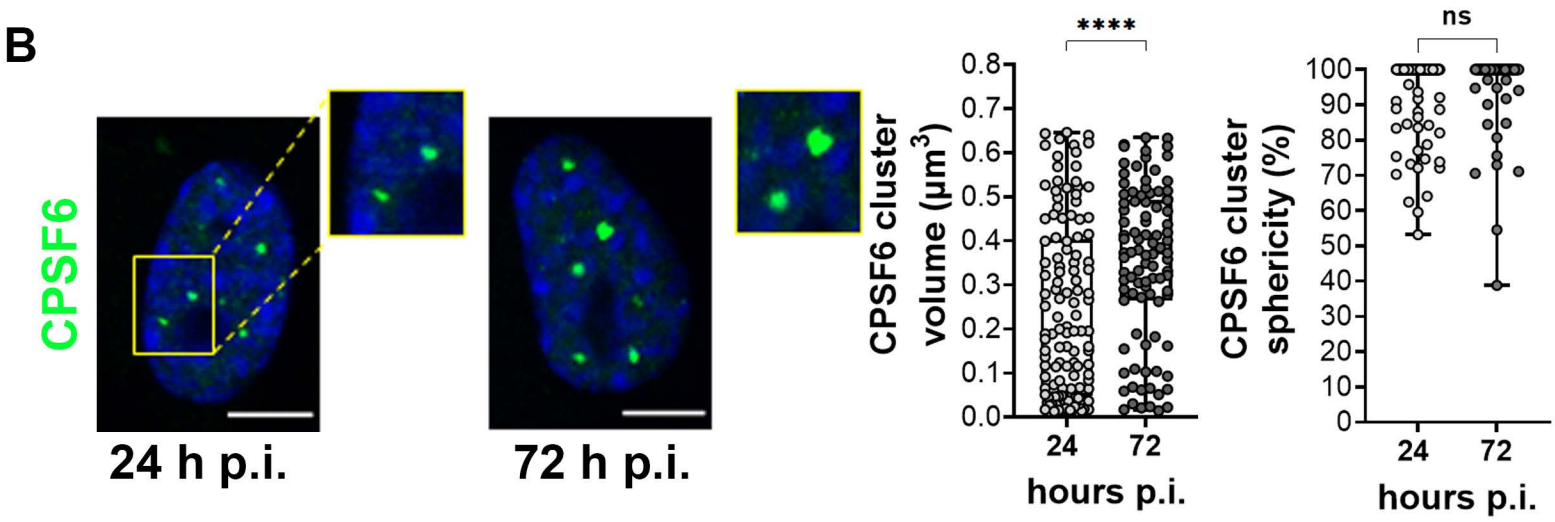

Sphericity	24 h p.i.	72 h p.i.
≥ 95%	99	81
< 95 %	26	14

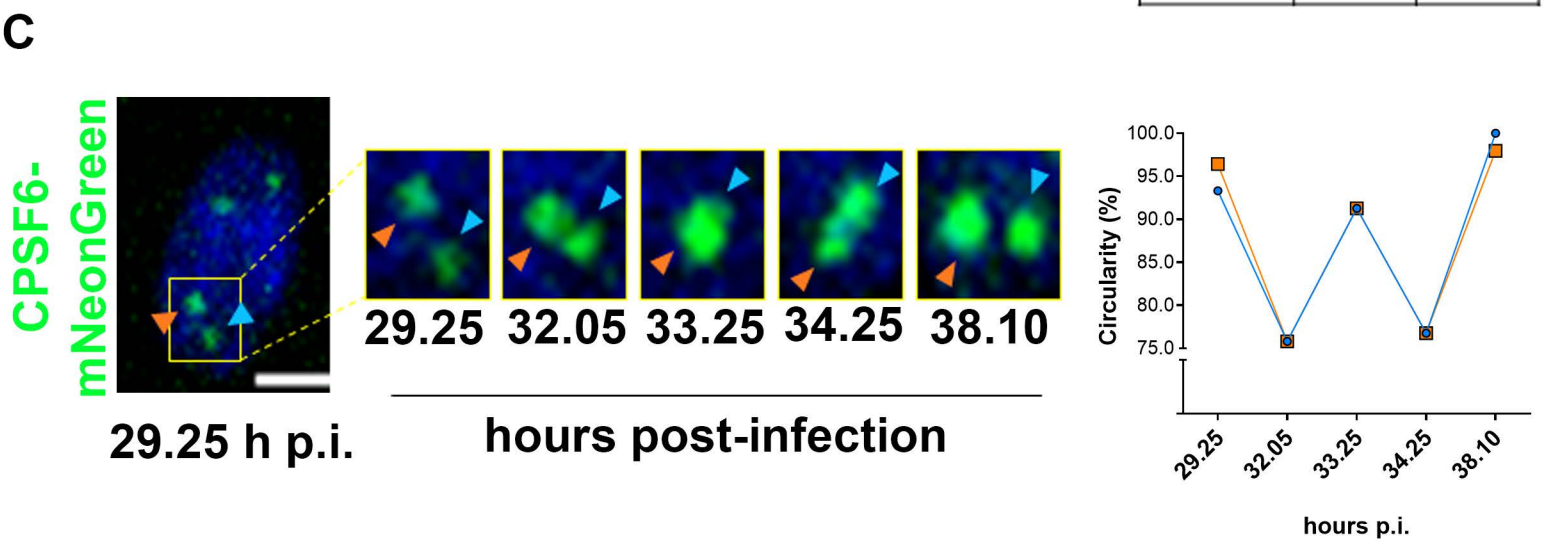

Figure 2

D

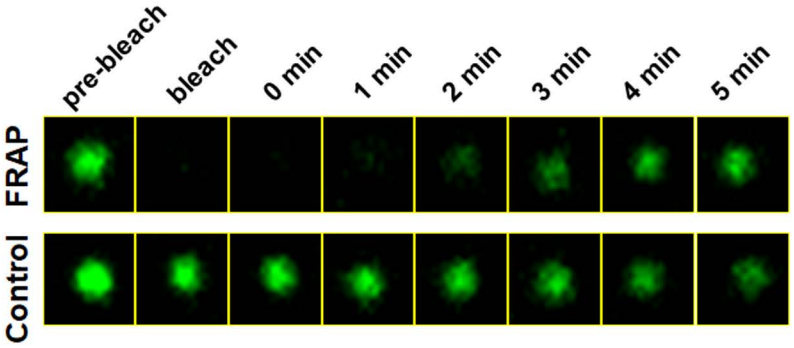

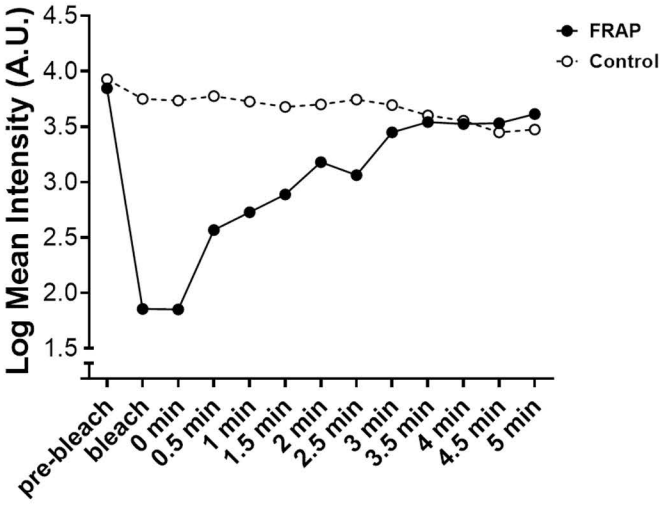

E

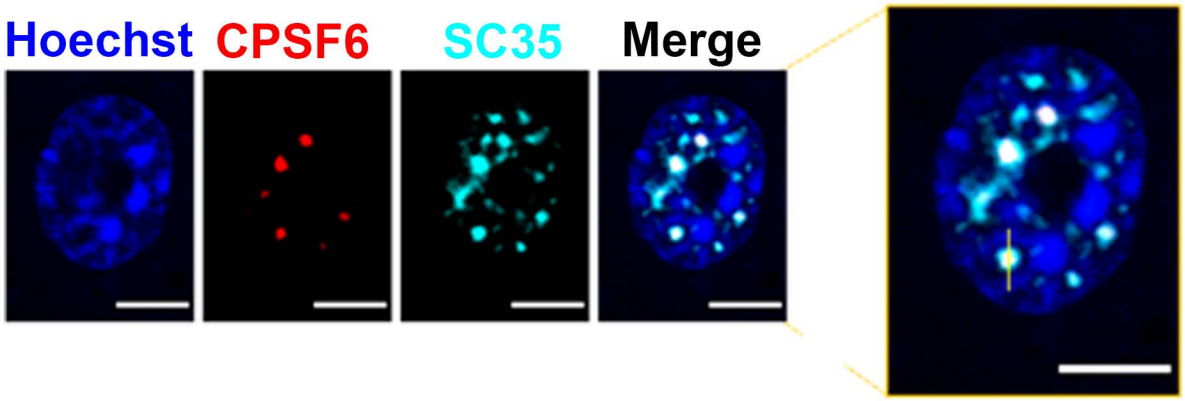

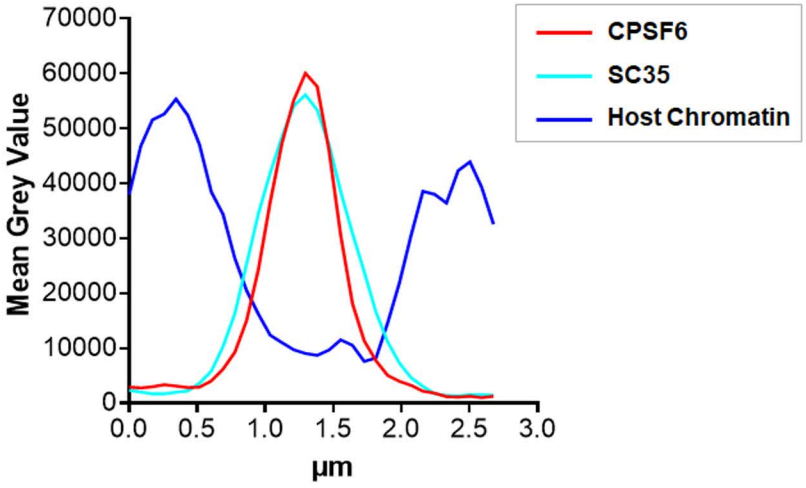

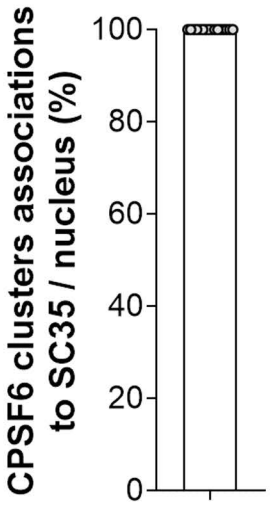

associated	92
unassociated	0

Figure 2

A

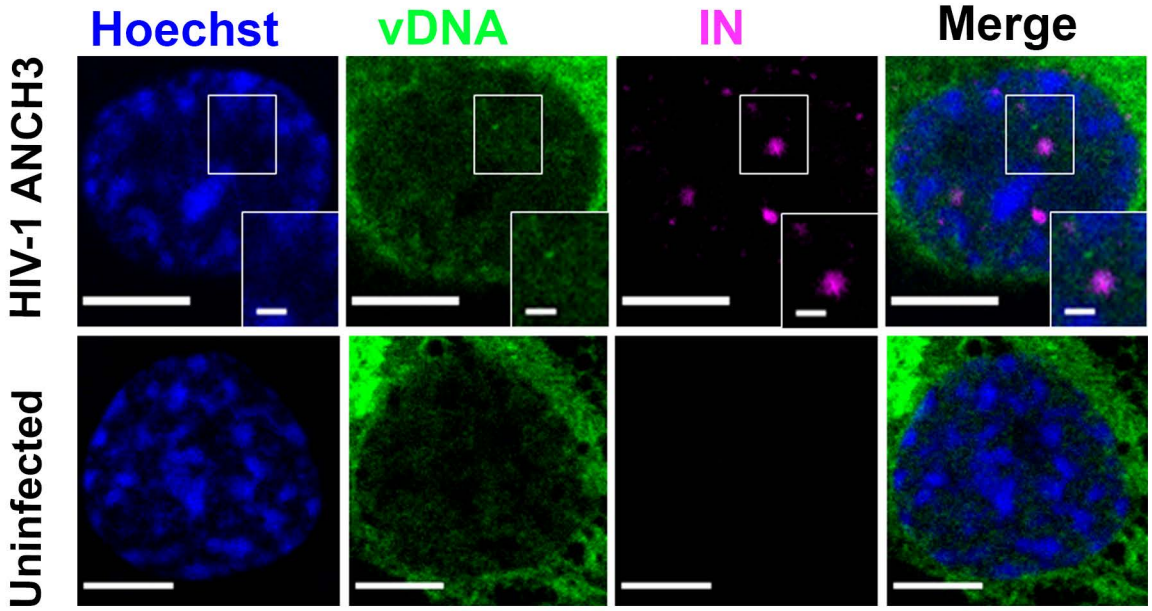

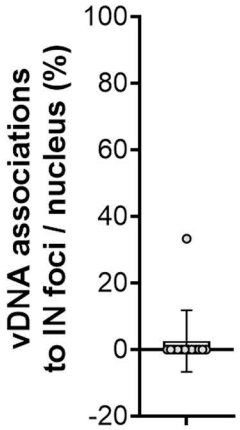

associated	1
unassociated	99

B

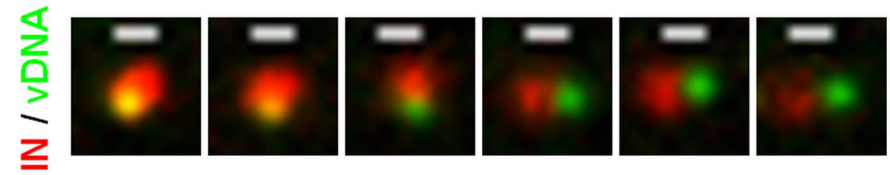

min 0 5 10 15 20 25

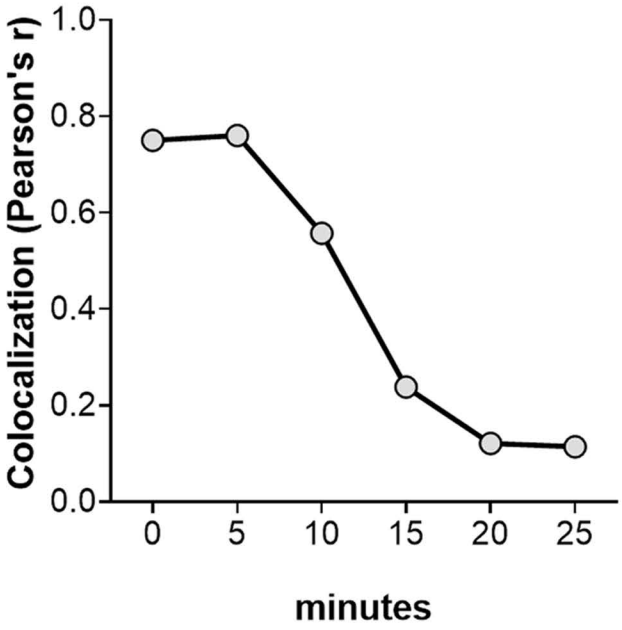

Figure 3

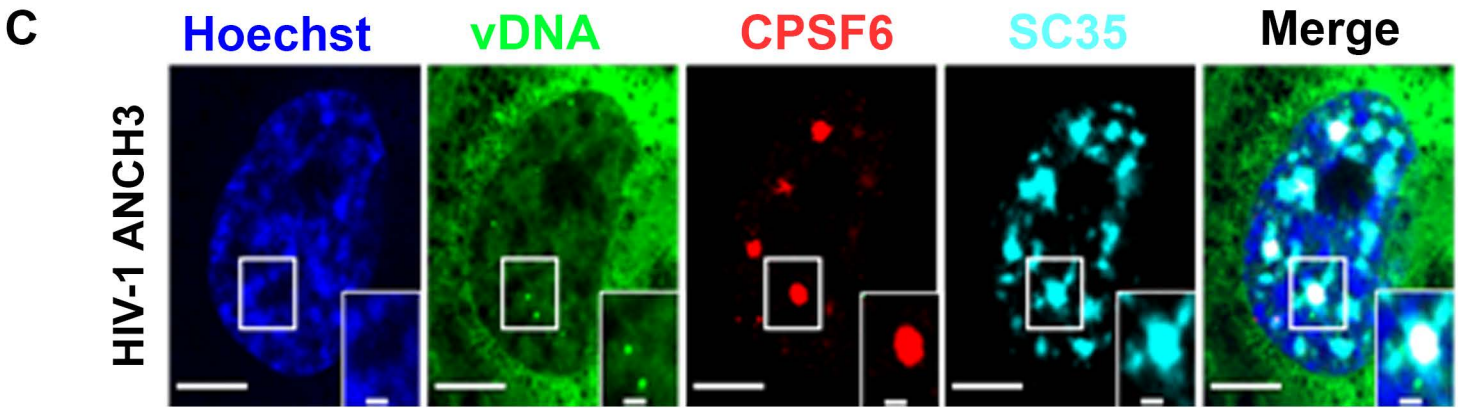

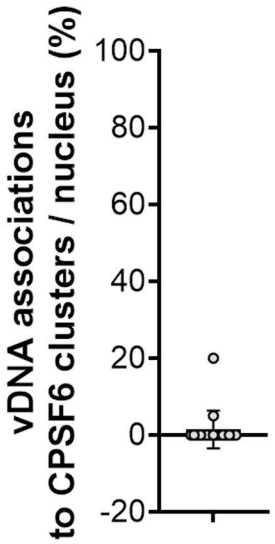

associated	2
unassociated	144

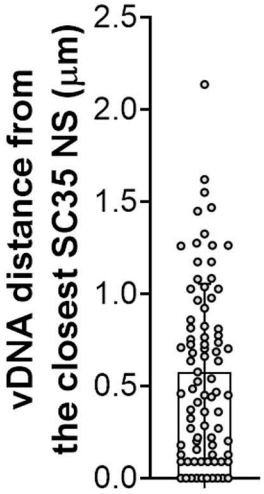

Figure 3

A

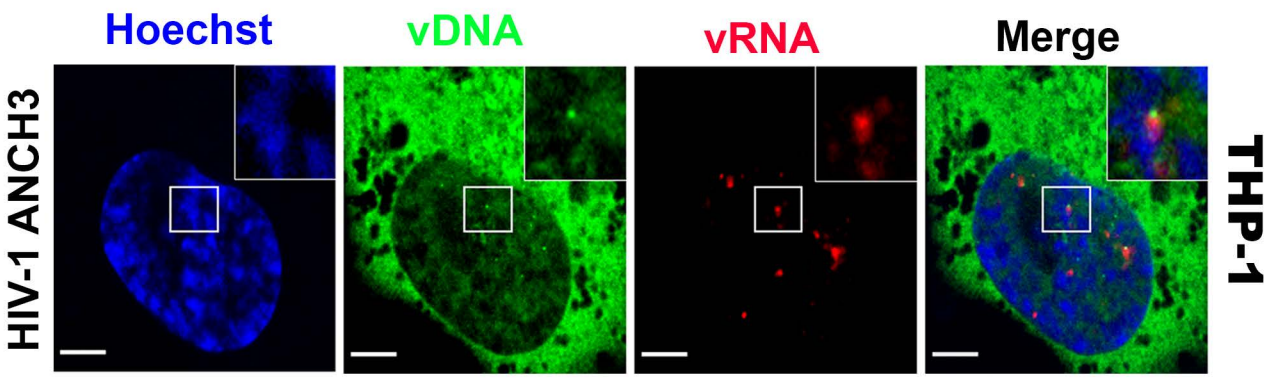

	vDNA to vRNA
associated	61
unassociated	99

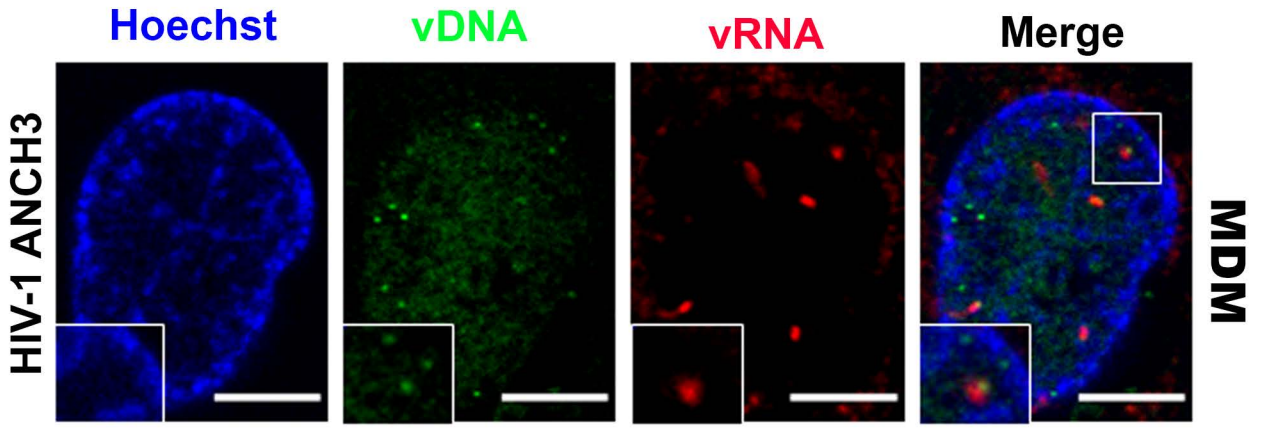

	vDNA to vRNA
associated	34
unassociated	19

Figure 4

B

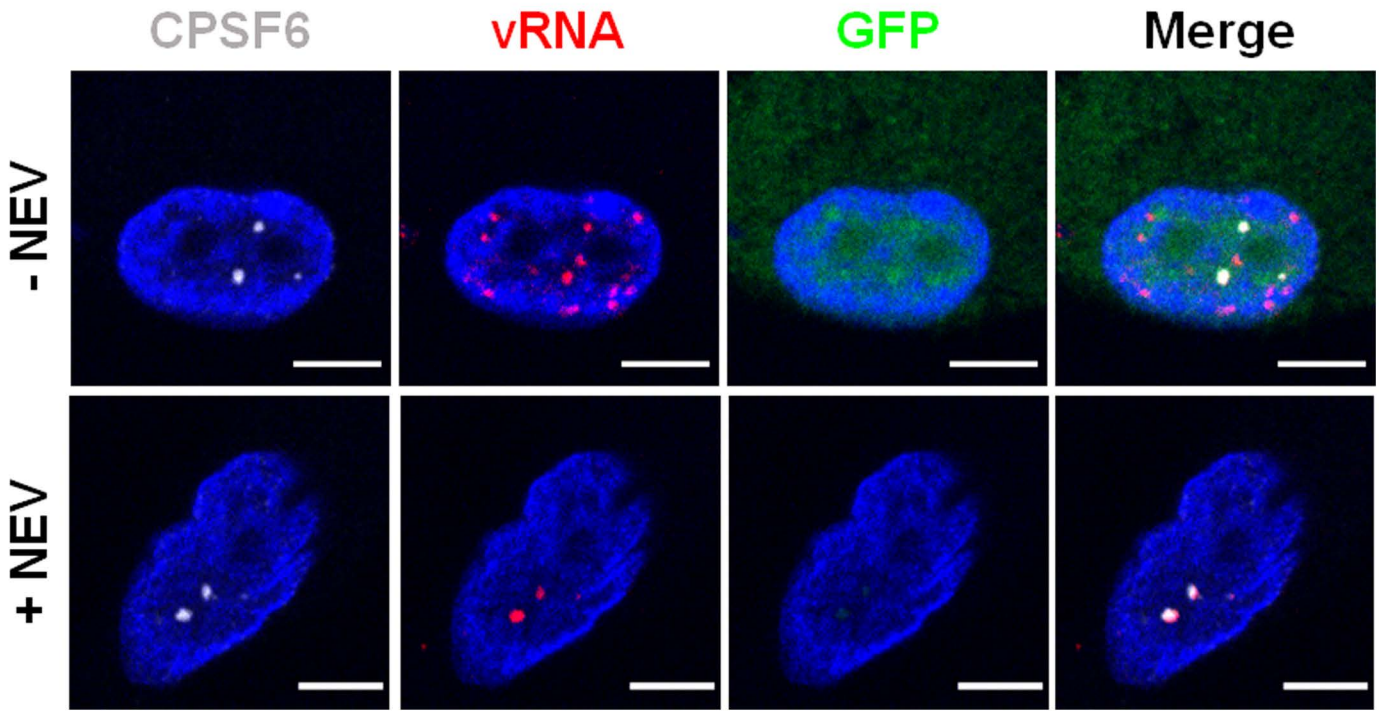

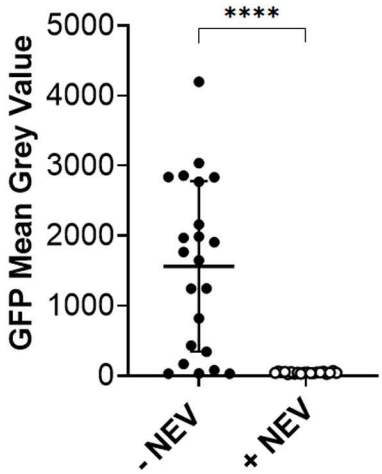

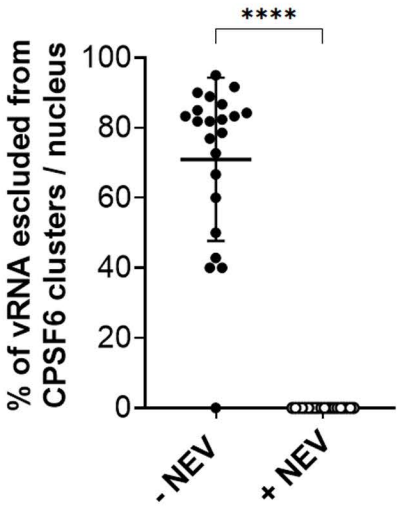

	- NEV	+ NEV
inside	56	66
outside	212	0

C

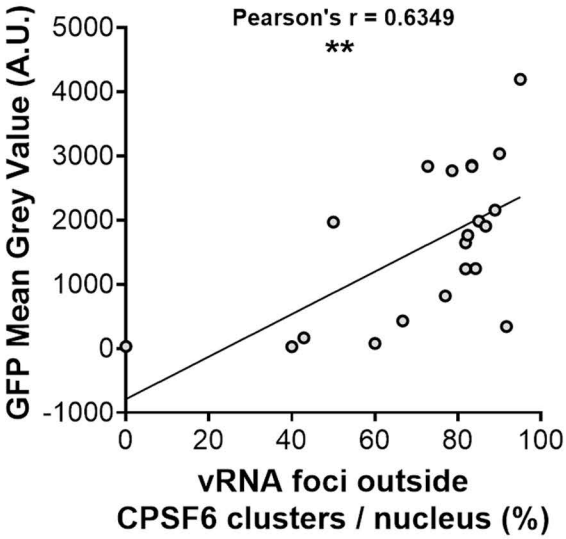

D

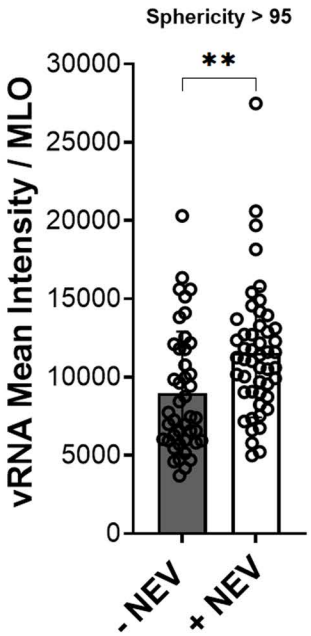

Figure 4

A

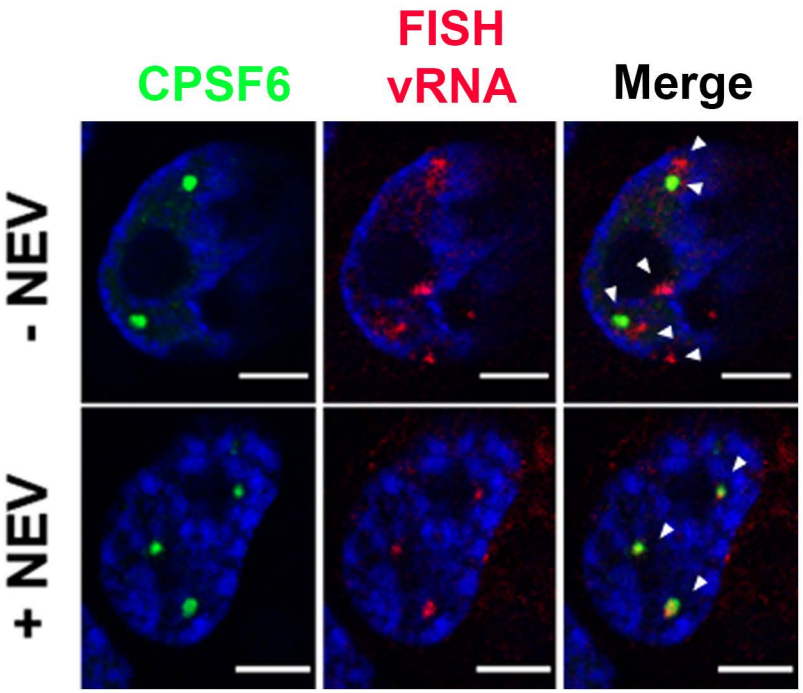

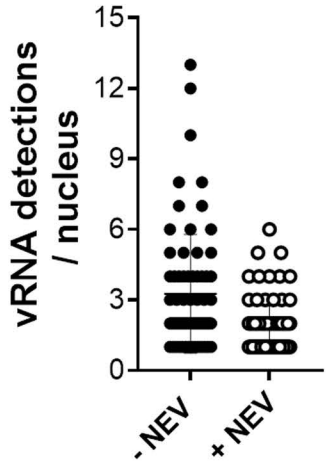

	- NEV	+ NEV
inside	117	129
outside	111	0

B

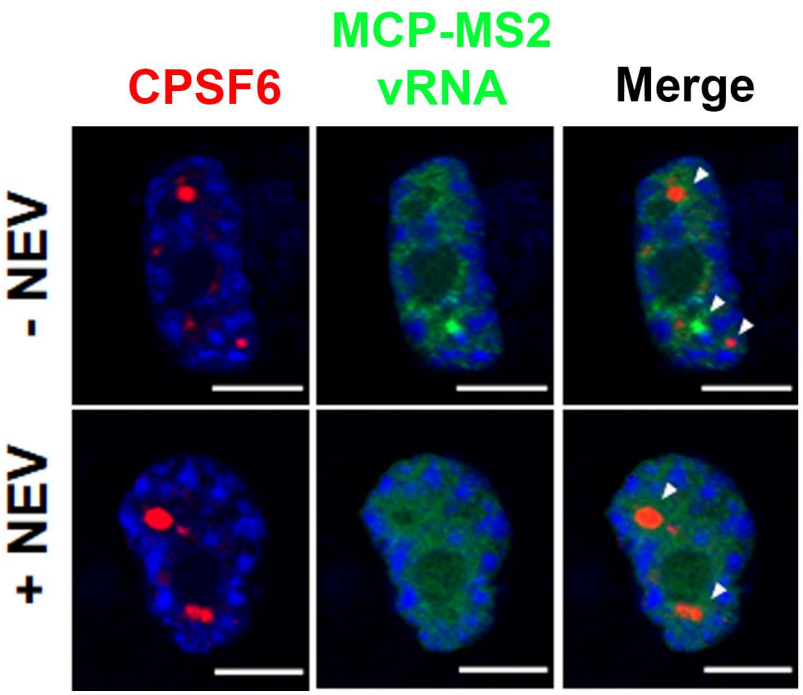

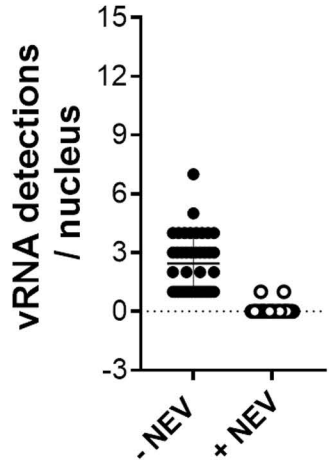

	- NEV	+ NEV
inside	0	0
outside	98	2

Figure 5

c

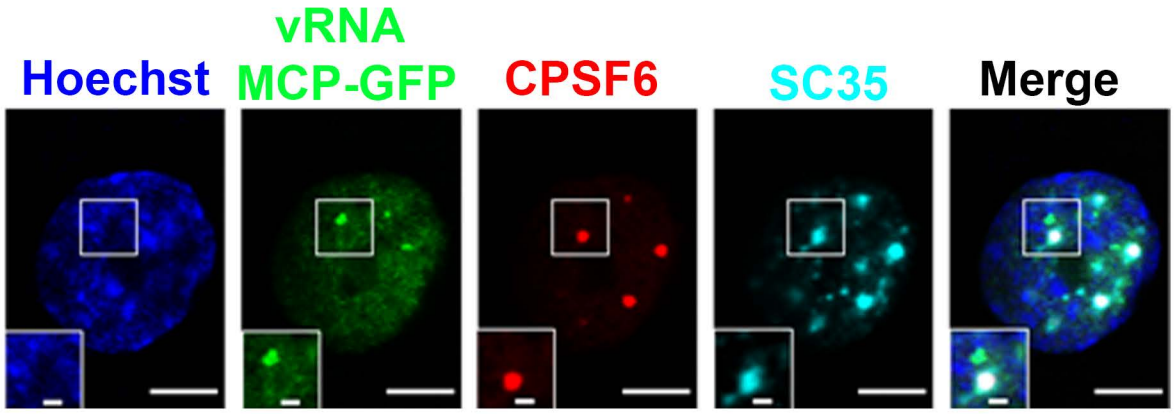
Hoechst
vRNA
MCP-GFP
CPSF6
SC35
Merge

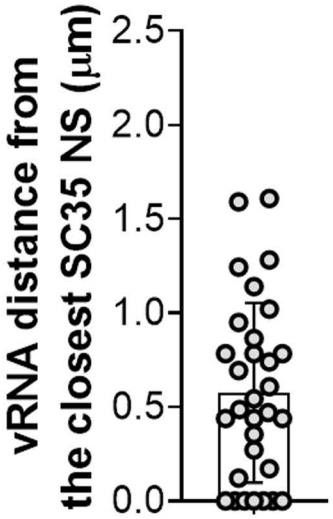
vRNA distance from
the closest SC35 NS (μm)
2.5
2.0
1.5
1.0
0.5
0.0

Figure 5

A

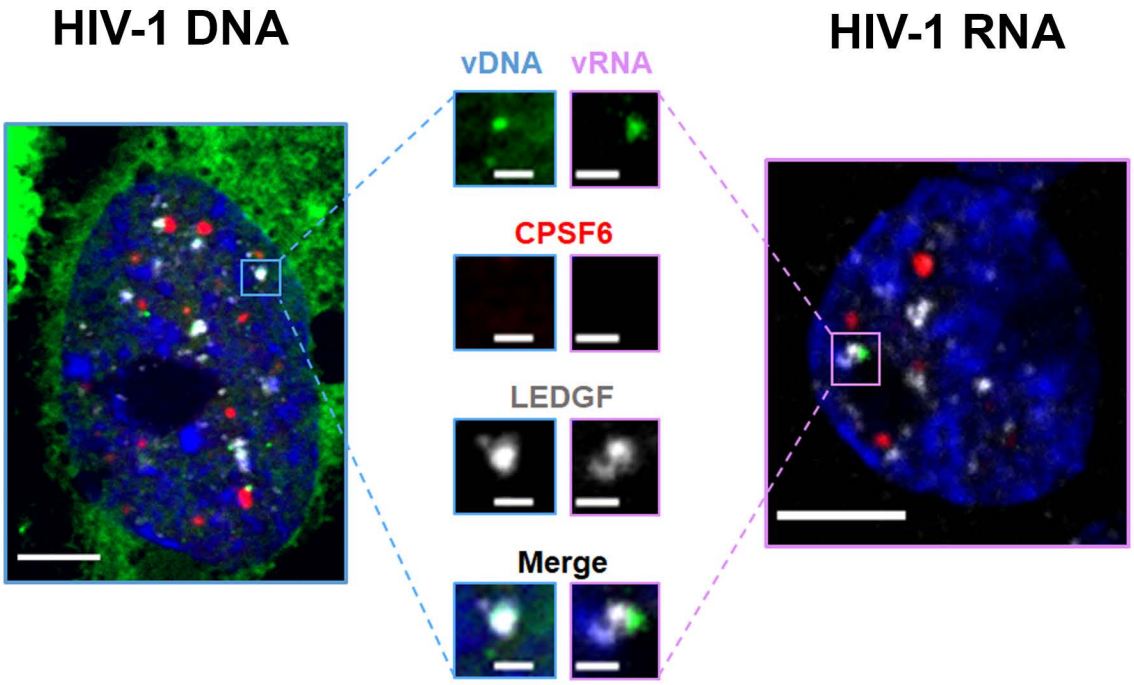

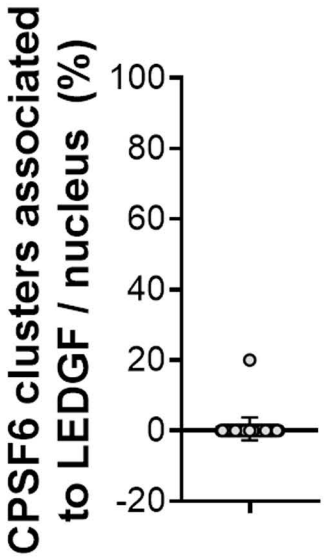

associatied	1
unassociated	160

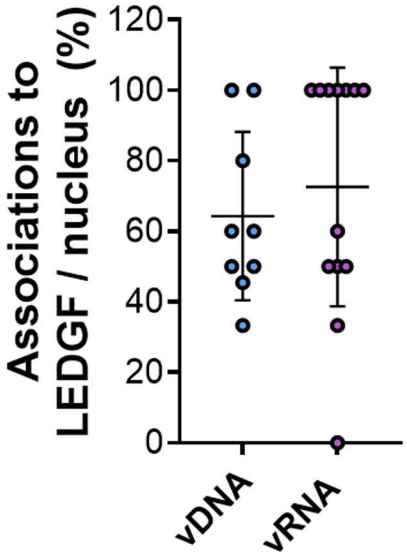

	vDNAs	vRNAs
associatied	33	15
unassociated	26	9

B

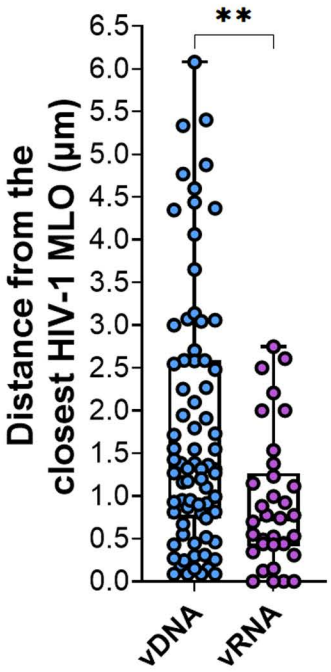

Figure 6

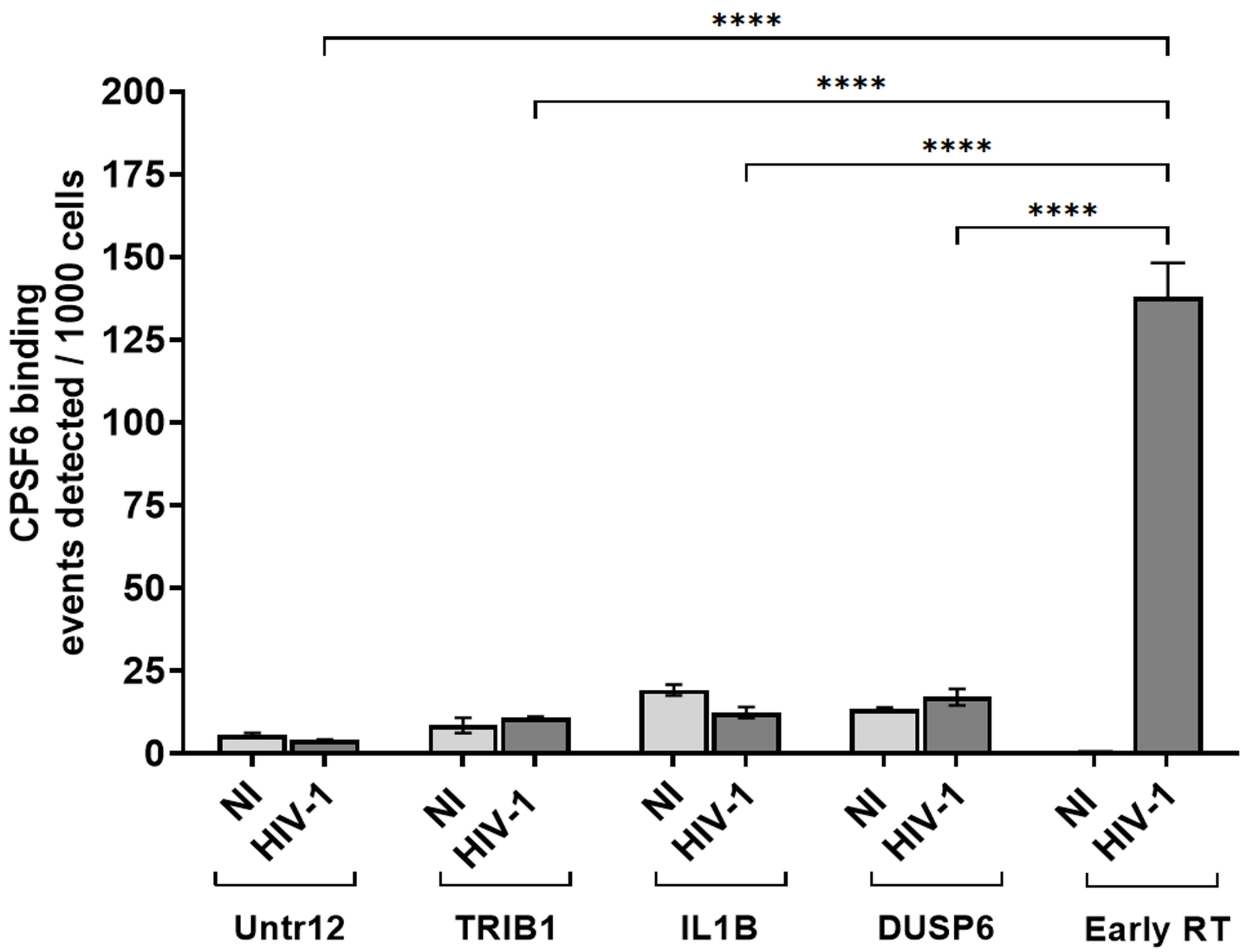
****
****
****
****
200
175
150
125
100
75
50
25
0
CPSF6 binding
events detected / 1000 cells
NI
HIV-1
NI
HIV-1
NI
HIV-1
NI
HIV-1
NI
HIV-1
Untr12
TRIB1
IL1B
DUSP6
Early RT

Figure S1

A

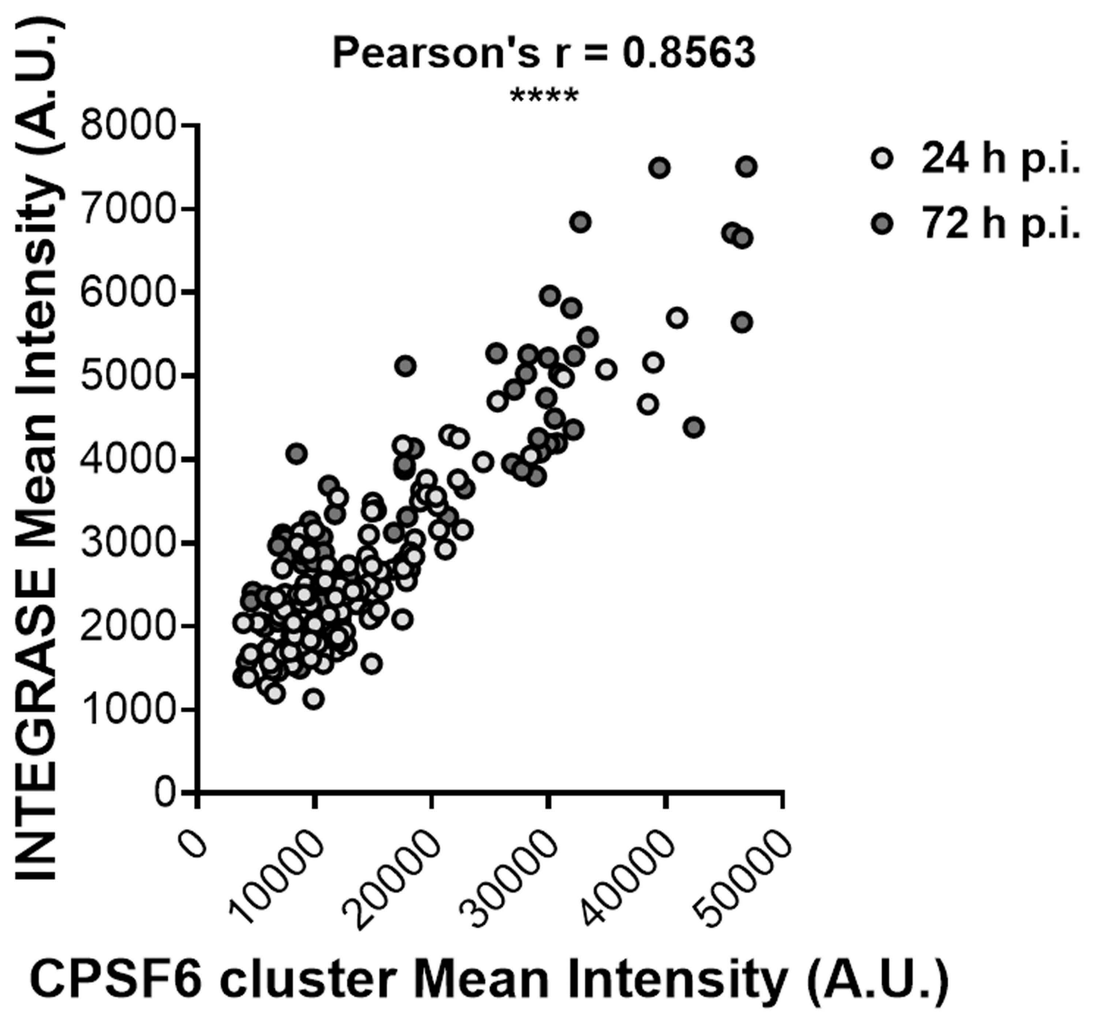
Pearson's r = 0.8563
****
INTEGRASE Mean Intensity (A.U.)
8000
7000
6000
5000
4000
3000
2000
1000
0
0
10000
20000
30000
40000
50000
CPSF6 cluster Mean Intensity (A.U.)
24 h p.i.
72 h p.i.

B

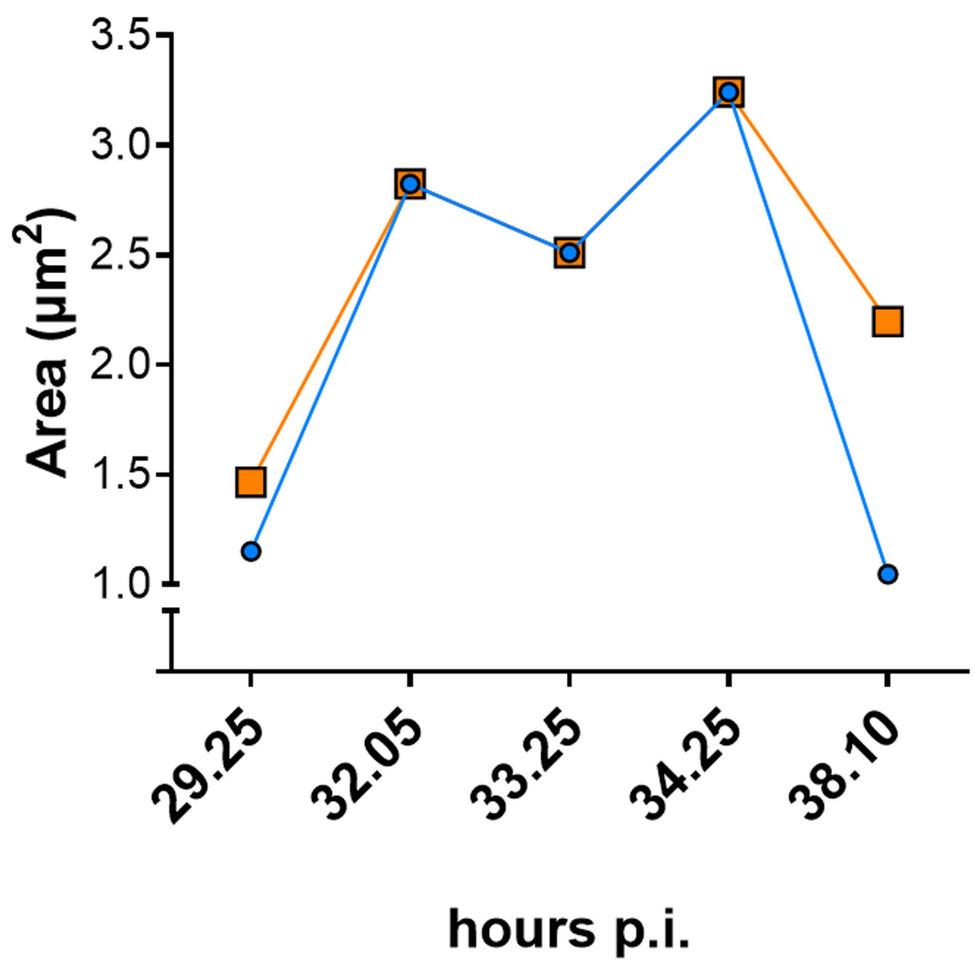
Area (µm²)
3.5
3.0
2.5
2.0
1.5
1.0
29.25
32.05
33.25
34.25
38.10
hours p.i.

Figure S2

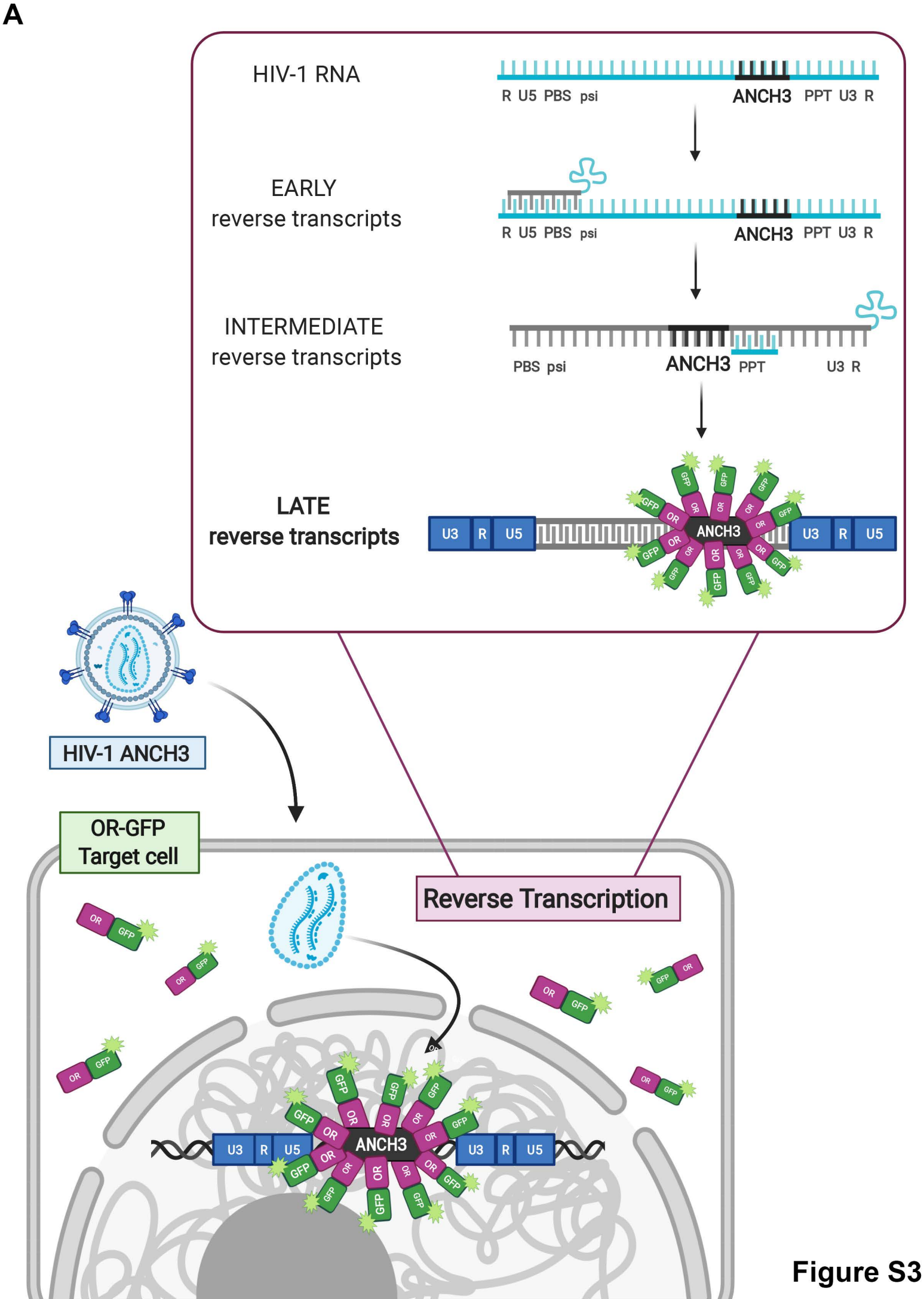
A
HIV-1 RNA
R U5 PBS psi
ANCH3
PPT U3 R
EARLY
reverse transcripts
R U5 PBS psi
ANCH3
PPT U3 R
INTERMEDIATE
reverse transcripts
PBS psi
ANCH3
PPT
U3 R
LATE
reverse transcripts
U3
R
U5
ANCH3
U3
R
U5
HIV-1 ANCH3
OR-GFP
Target cell
Reverse Transcription
OR
GFP
U3
R
U5
ANCH3
U3
R
U5

Figure S3

B

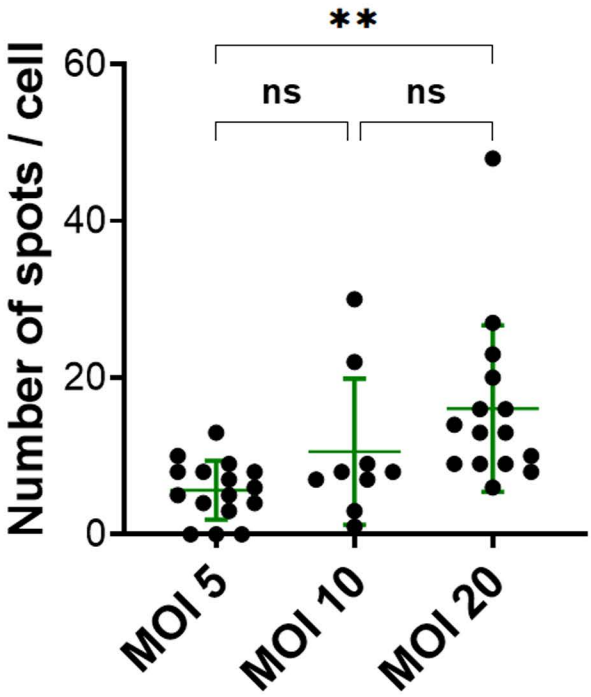
**
ns
ns
Number of spots / cell
60
40
20
0
MOI 5
MOI 10
MOI 20

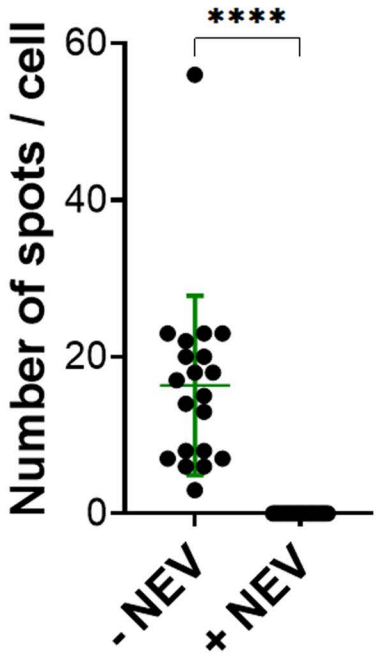
****
Number of spots / cell
60
40
20
0
- NEV
+ NEV

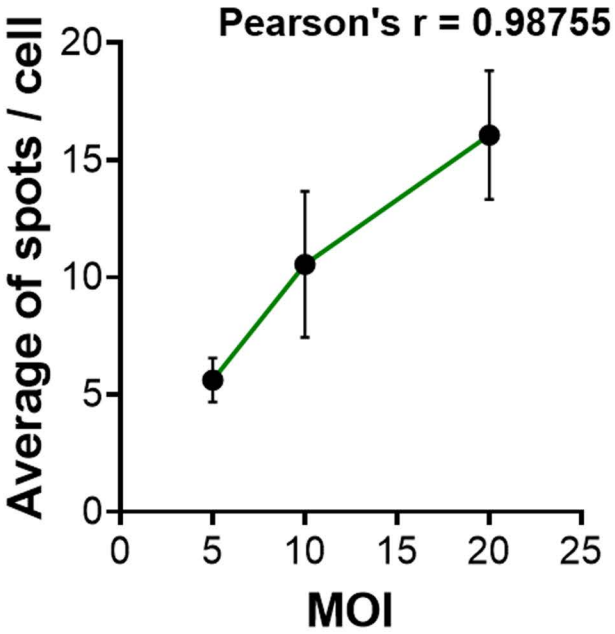
Pearson's r = 0.98755
Average of spots / cell
20
15
10
5
0
0
5
10
15
20
25
MOI

C

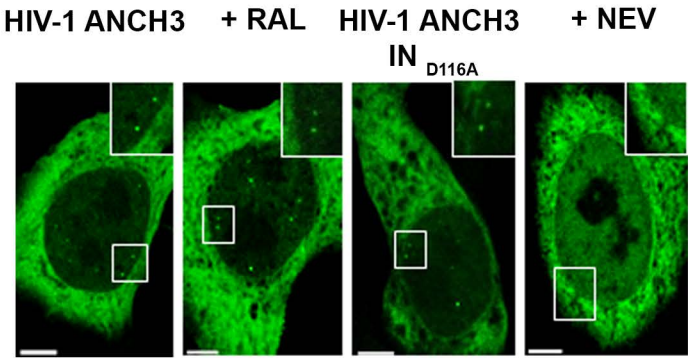
HIV-1 ANCH3
+ RAL
HIV-1 ANCH3 IN D116A
+ NEV

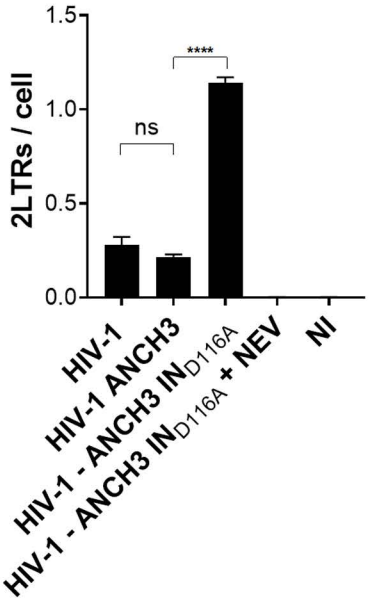
2LTRs / cell
1.5
1.0
0.5
0.0
ns
****
HIV-1
HIV-1 ANCH3
HIV-1 - ANCH3 IND116A
HIV-1 - ANCH3 IND116A + NEV
NI

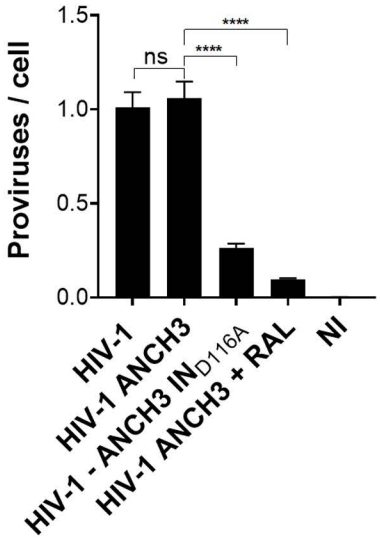
Proviruses / cell
1.5
1.0
0.5
0.0
ns
****
****
HIV-1
HIV-1 ANCH3
HIV-1 - ANCH3 IND116A
HIV-1 ANCH3 + RAL
NI

Figure S3

D **Clone HIV-1 ANCH3**

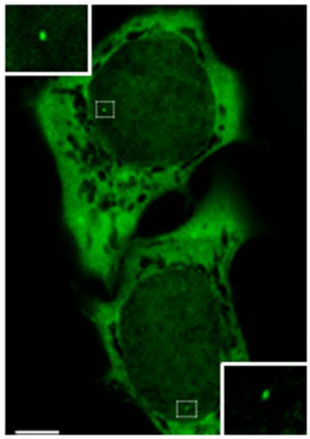

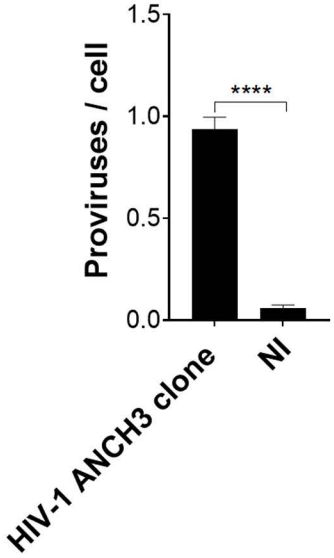

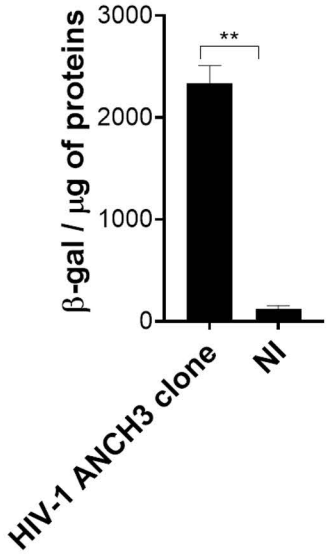

Figure S3

A

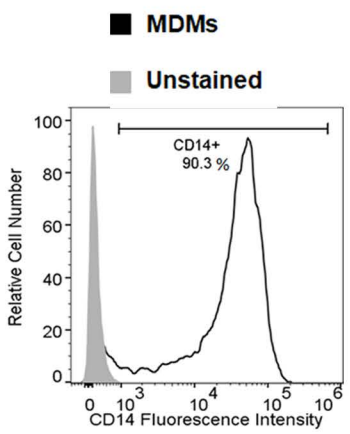

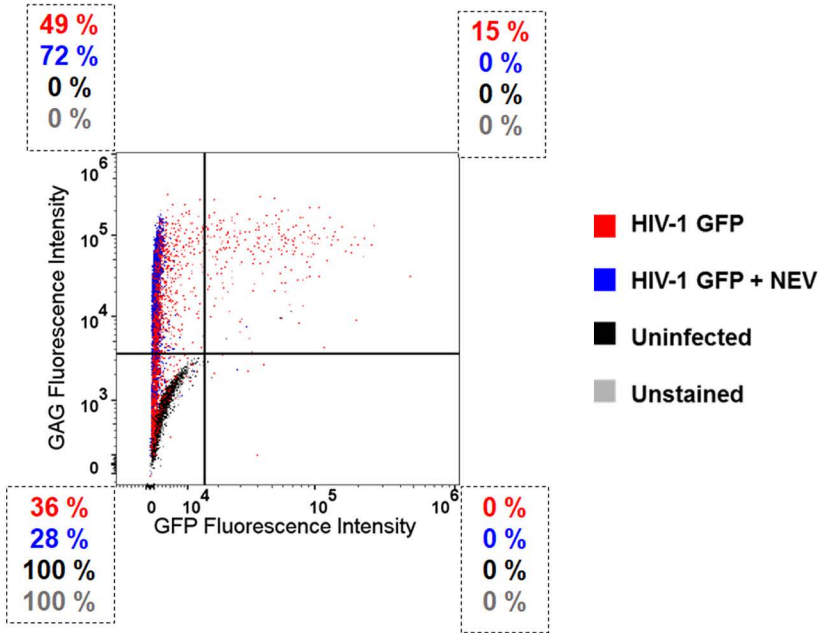

B

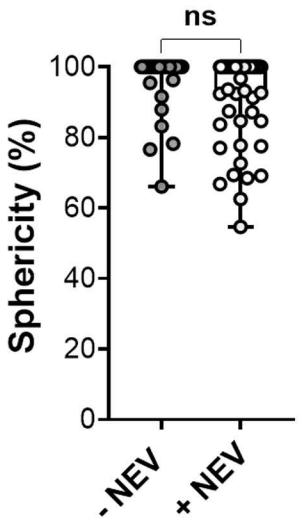

Sphericity	- NEV	+ NEV
≥ 95 %	43	49
< 95 %	6	21

C

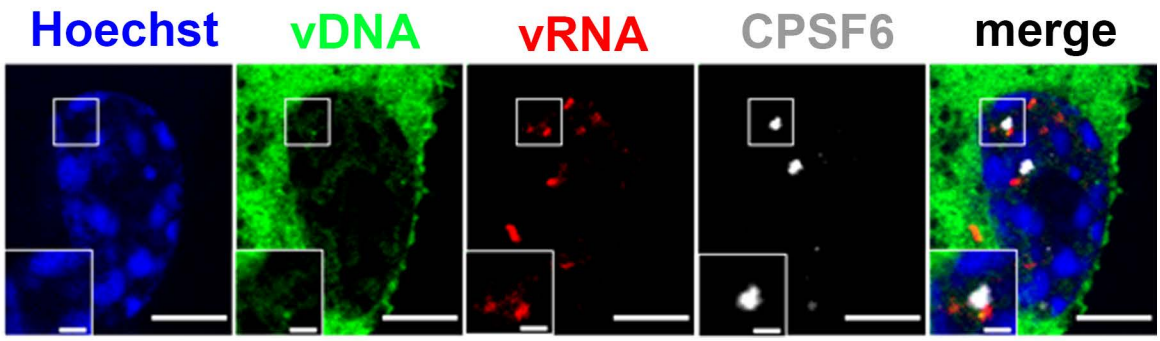

D

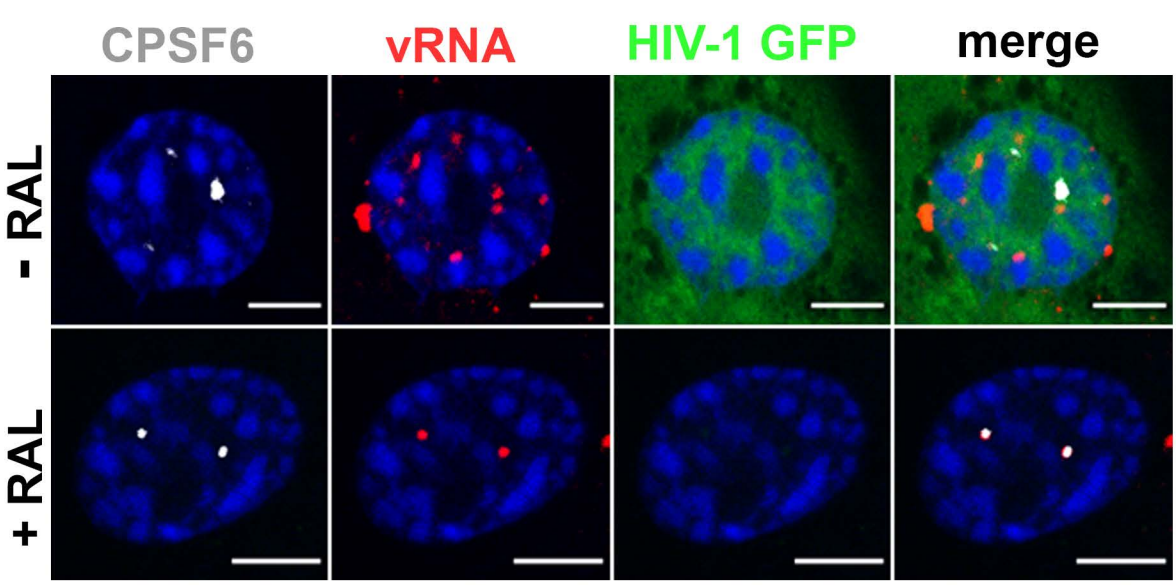

	- RAL	+ RAL
vRNAs inside CPSF6	91	112
vRNAs outside CPSF6	94	24

Figure S4

A

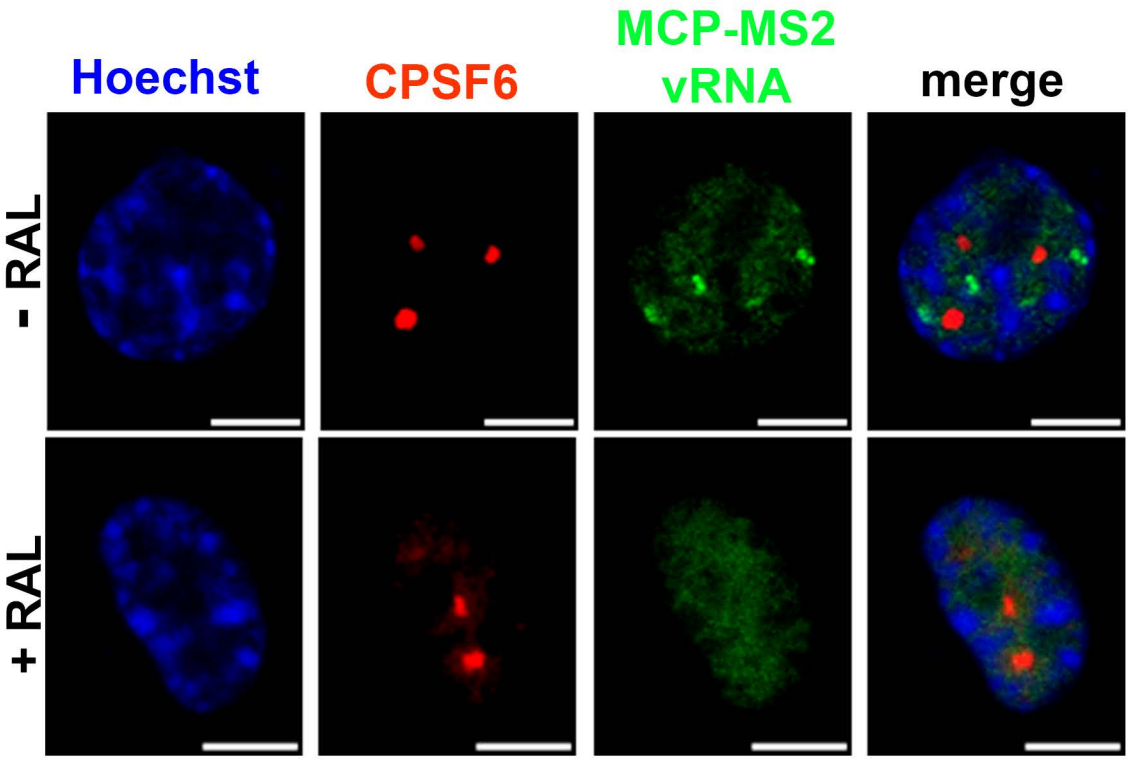

	- RAL	+ RAL
vRNAs inside CPSF6	0	0
vRNAs outside CPSF6	98	8

Figure S5

B

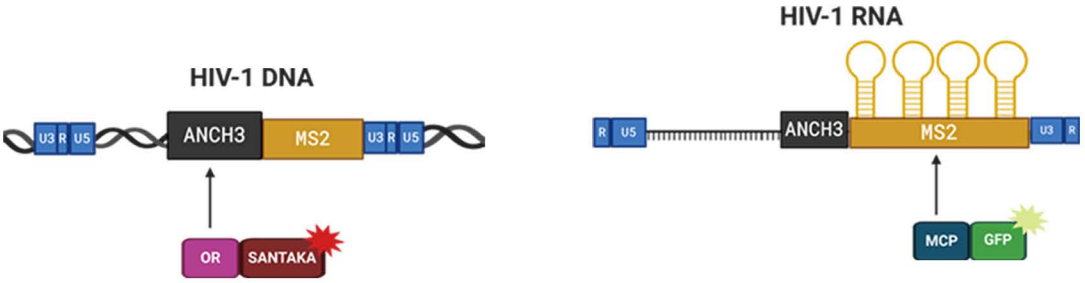

HIV-1 ANCH3 MS2 24 h post infection

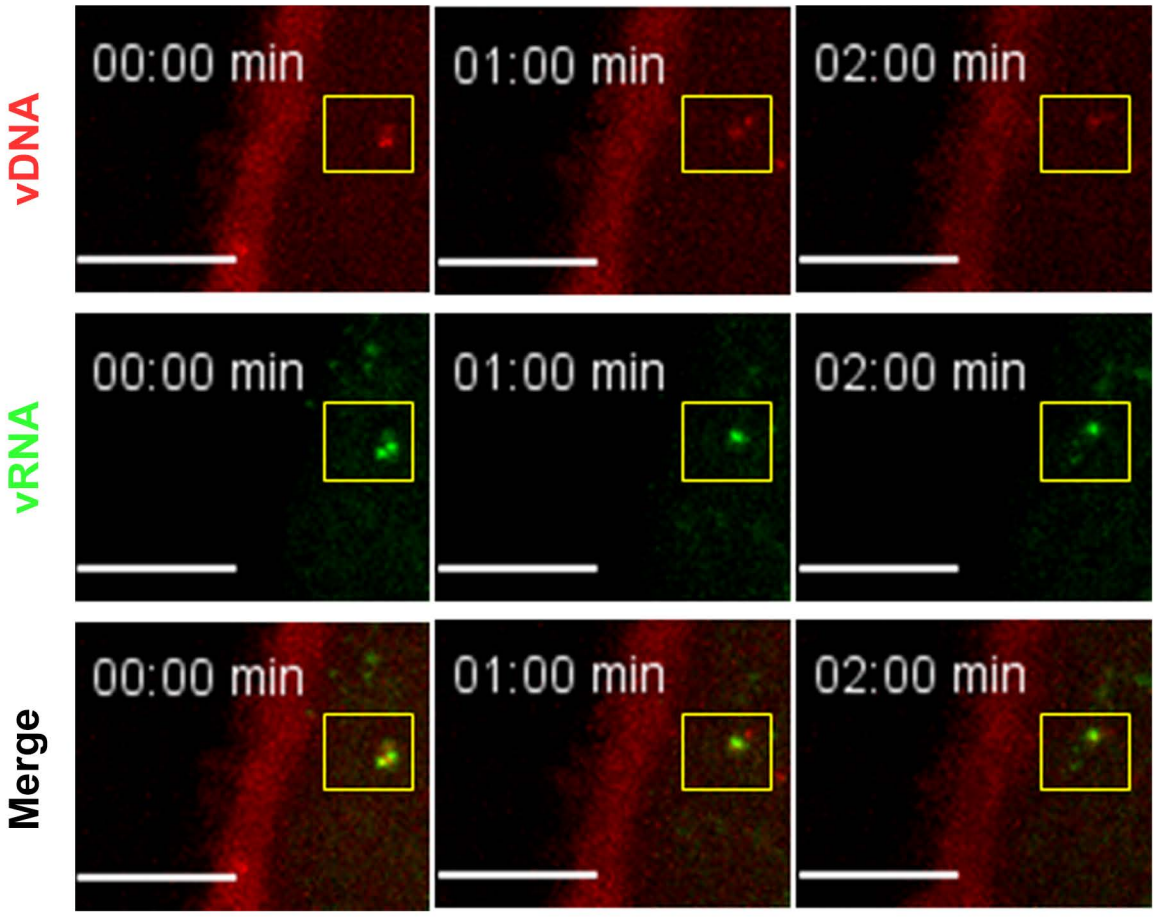

Figure S5

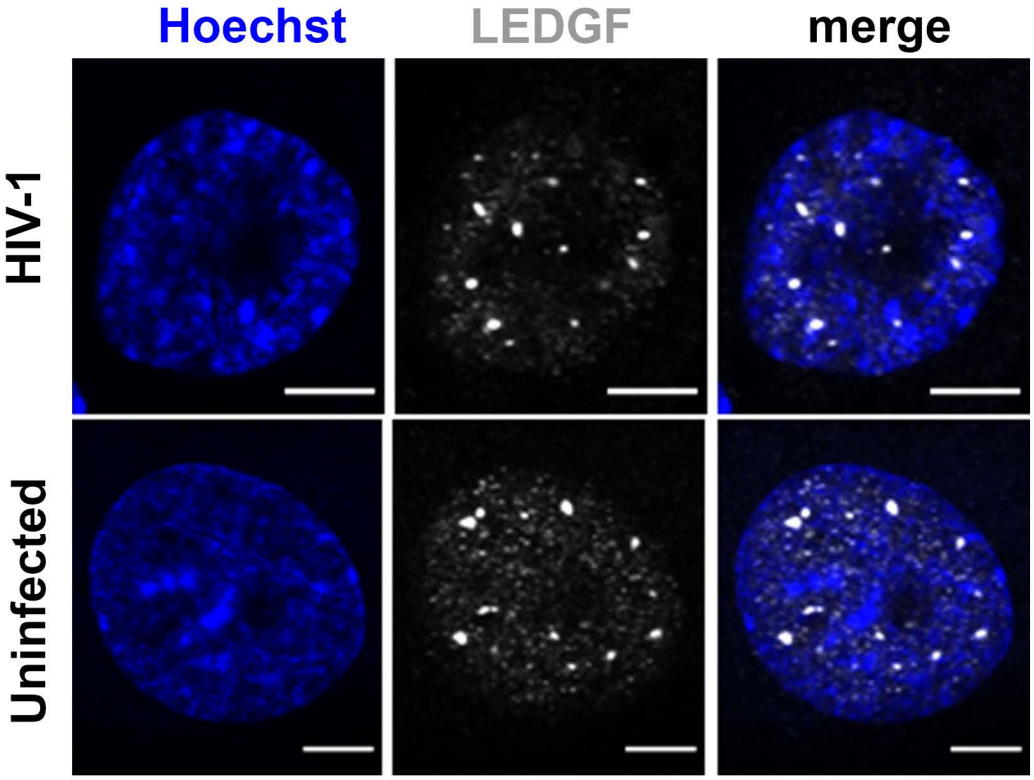
Hoechst
LEDGF
merge
HIV-1
Uninfected

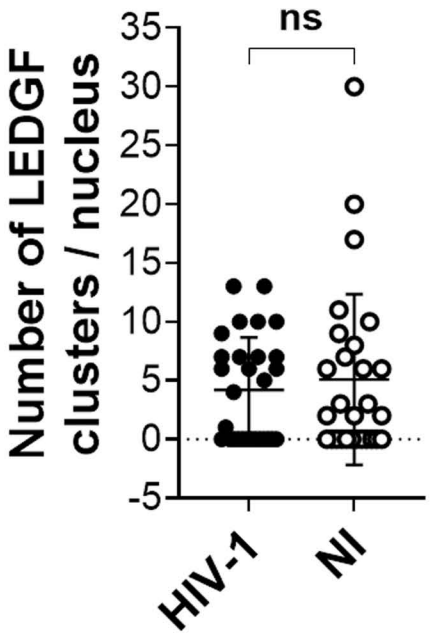
Number of LEDGF clusters / nucleus
35
30
25
20
15
10
5
0
-5
ns
HIV-1
NI

Figure S6

Probe Name	Sequence
HIV1-01	GGG GAT TGT AGG GAA TTC CAA ATT CCT GCT TTT ACA CTC GGA CCT CGT CGA CAT GCA TT
HIV1-02	CTT TTA GCT GAC ATT TAT CAC AGC TGG CTA TTA CAC TCG GAC CTC GTC GAC ATG CAT T
HIV1-03	GTG TGC TGG TAC CCA TGC CAG ATA GAC TTA CAC TCG GAC CTC GTC GAC ATG CAT T
HIV1-04	AAT ACT GGA GTA TTG TAT GGA TTT TCA GGC CCT TAC ACT CGG ACC TCG TCG ACA TGC ATT
HIV1-05	TTT TAC TGG TAC AGT CTC AAT AGG GCT AAT GGT TAC ACT CGG ACC TCG TCG ACA TGC ATT
HIV1-06	TAT GTT GAC AGG TGT AGG TCC TAC TAA TAC TGT TAC ACT CGG ACC TCG TCG ACA TGC ATT
HIV1-07	CTA ATC CTC ATC CTG TCT ACT TGC CAT TAC ACT CGG ACC TCG TCG ACA TGC ATT
HIV1-08	CAA TCA TCA CCT GCC ATC TGT TTT CCA TTT ACA CTC GGA CCT CGT CGA CAT GCA TT
HIV1-09	TTT CCA AAG TGG ATT TCT GCT GTC CCT GTA TTA CAC TCG GAC CTC GTC GAC ATG CAT T
HIV1-10	TTG TGG ATG AAT ACT GCC ATT TGT ACT GCT GTT ACA CTC GGA CCT CGT CGA CAT GCA TT
HIV1-11	TTA AGA TGT TCA GCC TGA TCT CTT ACC TGT TTA CAC TCG GAC CTC GTC GAC ATG CAT T
HIV1-12	TAC AGT CTA CTT GTC CAT GCA TGG CTT CTT ACA CTC GGA CCT CGT CGA CAT GCA TT
HIV1-13	TCA TGT TCA TCT TGG GCC TTA TCT ATT CCT TAC ACT CGG ACC TCG TCG ACA TGC ATT
HIV1-14	TGT CAG TTA GGG TGA CAA CTT TTT GTC TTC CTT TAC ACT CGG ACC TCG TCG ACA TGC ATT
HIV1-15	TGC TCC TAC TAT GGG TTC TTT CTC TAA CTT TAC ACT CGG ACC TCG TCG ACA TGC ATT
HIV1-16	TCT GTT AGT GCT TTG GTT CCT CTA AGG AGT TTT TAC ACT CGG ACC TCG TCG ACA TGC ATT
HIV1-17	CTG TAT GTC ATT GAC AGT CCA GCT GTC TTT TTT ACA CTC GGA CCT CGT CGA CAT GCA TT
HIV1-18	TGG CAG CAC TAT AGG CTG TAC TGT CCT TAC ACT CGG ACC TCG TCG ACA TGC ATT
HIV1-19	TCT GAT GTT TTT TGT CTG GTG TGG TAA GTC CCT TAC ACT CGG ACC TCG TCG ACA TGC ATT
HIV1-20	CCT CAA CAG ATG TTG TCT CAG CTC CTC TTA CAC TCG GAC CTC GTC GAC ATG CAT T
HIV1-21	ATT GCT GGT GAT CCT TTC CAT CCC TGT TAC ACT CGG ACC TCG TCG ACA TGC ATT
HIV1-22	TTT CTT TTT TAA CCC TGC GGG ATG TGG TAT TCT TAC ACT CGG ACC TCG TCG ACA TGC ATT
HIV1-23	TTT AAC TTT TGG GCC ATC CAT TCC TGG CTT ACA CTC GGA CCT CGT CGA CAT GCA TT
HIV1-24	CCC TAT CTT TAT TGT GAC GAG GGG TCG TTG TTA CAC TCG GAC CTC GTC GAC ATG CAT T

Table S1. Probes used for RNA FISH against HIV-1 pol

Supplementary Materials

Supplementary Figures Legend

Supplementary Figure S1. The histogram plot shows the number of copies ± SD of random genes in CPSF6 ChIP normalized for the input, compared to HIV-1 early reverse transcripts (RT) also normalized for the input (Fig. 1C). THP-1 cells infected with HIV-1 (MOI 5), 2 days p.i. One-way ANOVA followed by Tukey's multiple comparison test, ****=p ≤ 0.0001.

Supplementary Figure S2. A) Pearson's correlation of the mean intensity of CPSF6 clusters with the colocalizing IN focus (****=p ≤ 0.0001) in THP-1 cells infected with HIV-1 (MOI 5) + NEV (10 µM), 24h and 72 h p.i. 3D analysis. **B)** The graph shows the area along the memebraneless organelles fusion-fission event (video 1).

Supplementary Figure S3. A) Scheme of HIV-1 ANCHOR system created with BioRender.com. ANCH3 sequence has been cloned in the HIV-1 genome in place of Nef gene (HIV-1 ANCH3). The late retrotranscribed DNA of HIV-1 ANCH3 can be visualized in cells stably expressing the OR-GFP protein, thanks to OR accumulation on the double-stranded ANCH3 sequence. Viral DNA detection occurs mostly in the nucleus, where late reverse transcripts are abundant and are more likely to be exposed to the binding of OR-GFP. **B)** Analysis in HeLa P4R5 cells expressing OR-GFP infected with HIV-1 ANCH3, 24h p.i. The plots show: the vDNA spots count per cell for each MOI used and the comparison between the count in infected cells treated or not with NEV (10µM). Pearson's correlation of the average spots count with the increasing MOI used (n cells = 16, 9, 15) ± SEM. **C)** Confocal images of HeLa P4R5 cells expressing OR-GFP infected with HIV-1 ANCH3, HIV-1 ANCH3 + RAL (20 µM), HIV-1 ANCH3 IND116A and HIV-1 ANCH3 + NEV (10 µM) (MOI 30, 24 h p.i.). The histogram plots of 2-LTR circles and ALU-PCR represent the nuclear import and integration rates, respectively. One-way ANOVA followed by Tukey's multiple comparison test, ns=not-significant, ****=p ≤ 0.0001. **D)** Confocal image of HIV-1 ANCH3 provirus in an infected clone. On the right, histogram

plot of ALU-PCR and β-galactosidase expression in the infected clone compared to uninfected cells (NI). Unpaired t test, **=p ≤ 0.01, ****=p ≤ 0.0001.

Supplementary Figure S4. A) The FACS histogram displays CD14+ expression of the MDMs in this study. The FACS dot plot shows the correlation of GAG signal and GFP expression, with the related percentages per population (MOI 20, 2-3 days p.i.). **B)** Box plot of the sphericity of CPSF6 clusters in infected MDMs. Unpaired t test, ns=not-significant. **C)** Confocal image of Immuno-RNA FISH in THP-1 cell expressing OR-GFP infected with HIV-1 ANCH3 (MOI 20, 3 days p.i.). **D)** Confocal images of Immuno-RNA FISH in THP-1 cells infected with HIV-1 GFP ± RAL (20 µM) (MOI 10, 2 days p.i.). Scale bar: 5 µm, inset: 1 µm.

Supplementary Figure S5. A) Confocal images of THP-1 cells expressing MCP-GFP infected with HIV-1 ANCH3 MS2 ± RAL (20µM), (MOI 2.5, 3 days p.i.). **B)** The cartoon model shows the double labelling system: the HIV-1 genome is tagged both with ANCH3 and MS2 sequences. The differently fluorescent reporters allow the simultaneous detection of vDNA through the binding of OR-GFP to ANCH3 sequence and of vRNA through the binding of MCP to MS2 stem loops. Created with BioRender.com. **B)** Frames from a time-lapse microscopy of HeLa MCP-GFP cells transduced with OR-SANTAKA LV (MOI 1) and 48 hours after infected with HIV-1 ANCH3 MS2 (MOI 50), 24 h p.i.. Projection of 6 Z slices, spacing 0.2 µm with Ti2E inverted microscope (Nikon), based on a CSU-W1 spinning-disk (Yokogawa), using a 60X objective (Plan Apochromat, oil immersion, NA=1.4). Scale bar: 5 µm.

Supplementary Figure S6. A) Confocal images of THP-1 cells infected with HIV-1 (MOI10, 3 days p.i.) compared to uninfected cells. The scatter plot shows the count of LEDGF clusters per nucleus (n = 29 cells (HIV-1), 28 cells (NI)); unpaired t test, ns = not-significant, Scale bar: 5 µm.

Video Legends

Video 1. CPSF6 clusters dynamics in HIV-1 infected cells. Time-lapse microscopy of THP-1 cells expressing CPSF6 mNeonGreen infected with HIV-1 (MOI 10). Time post infection is indicated on the top. It is possible to appreciate 2 fusion events. Representative of 6 independent experiments. Scale bar: 5 µm.

Video 2. FRAP time lapse of CPSF6 clusters in HIV-1 infected cells. FRAP time-lapse in THP-1 cells expressing CPSF6 mNeonGreen infected with HIV-1 (MOI 10, 3 days p.i.). The first 3 frames are pre-bleaching, frame 4 is the bleach and from frame 5 it starts the recovery. Representative of 3 independent experiments. Scale bar: 5 µm.

Video 3. Generation and separation of ds vDNA from the IN focus in live. Time-lapse in HeLa P4R5 cells infected with HIV-1 ANCH3 IN_{D116A} GIR virus (MOI 50, 13.30 h p.i.). The vDNA (green) signal generates from the integrase (IN) proteins (red). The video is a Z projection of 4 slices, spacing 0.4 µm. Scale bar: 5 µm.

Video 4. Separation of ds vDNA from IN focus in live. Time-lapse in HeLa P4R5 cells infected with HIV-1 ANCH3 IN_{D116A} GIR virus (MOI 50, 18 h p.i.). On the left, the vDNA (green) separates along time from the integrase (IN) proteins (red). On the right, an example of vDNA and IN proteins separated in the nuclear space. The video is a Z projection of 4 slices, spacing 0.4 µm. Scale bar: 5 µm.